Available online at www.sciencedirect.com

ScienceDirect

Geochimica et Cosmochimica Acta 246 (2019) 174–196

Geochimica et Cosmochimica Acta

www.elsevier.com/locate/gca

Impact of natural re-oxygenation on the sediment dynamics of manganese, iron and phosphorus in a euxinic Baltic Sea basin

Martijn Hermans [a,*], Wytze K. Lenstra [a], Niels A.G.M. van Helmond [a] Thilo Behrends [a], Matthias Egger [a,1], Marie J.M. Séguret [a], Erik Gustafsson [b] Bo G. Gustafsson [b,c], Caroline P. Slomp [a]

[a] *Department of Earth Sciences (Geochemistry), Faculty of Geosciences, Utrecht University, P.O. Box 80.021, 3508 TA Utrecht, the Netherlands*
[b] *Baltic Nest Institute, Baltic Sea Centre, Stockholm University, SE-106 91 Stockholm, Sweden*
[c] *Tvärminne Zoological Station, University of Helsinki, J.A. Palménin tie 260, Hanko, Uusimaa, Finland*

Received 18 June 2018; accepted in revised form 22 November 2018; available online 26 November 2018

Abstract

The Baltic Sea is characterized by the largest area of hypoxic (oxygen (O_2) < 2 mg L^{-1}) bottom waters in the world's ocean induced by human activities. Natural ventilation of these O_2-depleted waters largely depends on episodic Major Baltic Inflows from the adjacent North Sea. In 2014 and 2015, two such inflows led to a strong rise in O_2 and decline in phosphate (HPO_4^{2-}) in waters below 125 m depth in the Eastern Gotland Basin. This provided the opportunity to assess the impact of such re-oxygenation events on the cycles of manganese (Mn), iron (Fe) and phosphorus (P) in the sediment for the first time. We demonstrate that the re-oxygenation induced the activity of sulphur (S)-oxidising bacteria, known as *Beggiatoaceae* in the surface sediment where a thin oxic and suboxic layer developed. At the two deepest sites, strong enrichments of total Mn and to a lesser extent Fe oxides and P were observed in this surface layer. A combination of sequential sediment extractions and synchrotron-based X-ray spectroscopy revealed evidence for the abundant presence of P-bearing rhodochrosite and Mn(II) phosphates. In contrast to what is typically assumed, the formation of Fe oxides in the surface sediment was limited. We attribute this lack of Fe oxide formation to the high flux of reductants, such as sulphide, from deeper sediments which allows Fe (II) in the form of FeS to be preserved and restricts the penetration of O_2 into the sediment. We estimate that enhanced P sequestration in surface sediments accounts for only ~5% of water column HPO_4^{2-} removal in the Eastern Gotland Basin linked to the recent inflows. The remaining HPO_4^{2-} was transported to adjacent areas in the Baltic Sea. Our results highlight that the benthic O_2 demand arising from the accumulation of organic-rich sediments over several decades, the legacy of hypoxia, has major implications for the biogeochemical response of euxinic basins to re-oxygenation. In particular, P sequestration in the sediment in association with Fe oxides is limited. This implies that artificial ventilation projects that aim at removing water column HPO_4^{2-} and thereby improving water quality in the Baltic Sea will likely not have the desired effect.

Keywords: Manganese; Iron; Phosphorus; Re-oxygenation; Baltic Sea; Major Baltic Inflow

* Corresponding author.
E-mail addresses: m.hermans@uu.nl (M. Hermans), w.k.lenstra@uu.nl (W.K. Lenstra), n.vanhelmond@uu.nl (N.A.G.M. van Helmond), t.behrends@uu.nl (T. Behrends), matthias.egger@theoceancleanup.com (M. Egger), m.j.m.seguret@uu.nl (M.J.M. Séguret), erik.gustafsson@su.se (E. Gustafsson), bo.gustafsson@su.se (B.G. Gustafsson), c.p.slomp@uu.nl (C.P. Slomp).
[1] Now at: The Ocean Cleanup, Batavierenstraat 15, 3014 JH Rotterdam, South Holland, the Netherlands.

https://doi.org/10.1016/j.gca.2018.11.033
0016-7037/

1. INTRODUCTION

Oxygen (O_2) depletion in marine environments is increasing worldwide (Diaz and Rosenberg, 2008; Altieri et al. 2017; Schmidtko et al., 2017). In coastal systems, bottom water hypoxia ($O_2 < 2$ mg L^{-1}; <63 μM) and anoxia ($O_2 = 0$ mg L^{-1}) can result in areas known as 'dead zones', characterized by mass mortality of marine life due to the lack of O_2 and, in some cases, by the presence of highly toxic hydrogen sulphide (H_2S) (euxinia; Diaz and Rosenberg, 2008). The spatial extent of these dead zones has increased drastically in coastal marine waters since the 1960s (Diaz and Rosenberg, 2008). Furthermore, hypoxia and anoxia have greatly altered the sedimentary cycles of key nutrients, such as manganese (Mn), iron (Fe), phosphorus (P) and nitrogen (N) in many coastal systems (Ingall and Jahnke, 1994; Vahtera et al., 2007; Howarth et al., 2011; Lenz et al., 2015).

The semi-enclosed brackish Baltic Sea is the world's largest human-induced hypoxic/anoxic water mass (Carstensen et al., 2014a). While hypoxia/anoxia was restricted to a surface area of ~10,000 km^2 before 1950, the O_2-depleted areas expanded to more than 60,000 km^2 in recent years due to eutrophication and global warming (e.g. Carstensen et al., 2014b). The Baltic Sea is naturally susceptible to hypoxia because submarine sills limit horizontal water exchange, also with the adjacent North Sea, and pronounced vertical stratification in the water column prevents the supply of O_2 to waters below the permanent halocline, which is located at 60–80 m water depth in the Central Baltic (Mohrholz et al., 2015).

Natural ventilation of deeper waters in the Baltic Sea depends on large-scale episodic inflow events of oxygenated waters from the North Sea. Such episodic events, so-called Major Baltic Inflows (MBIs) are regulated by wind and air pressure related variations in sea level (Gustafsson and Andersson, 2001). During MBIs substantial amounts of saline and O_2-rich water enter the Baltic Sea through the Danish Straits and subsequently ventilate the deeper basins. However, the inflow of saline water enhances stratification, ultimately resulting in reduced vertical mixing of O_2 across the halocline, thereby contributing to the expansion of hypoxia (Conley et al., 2002). Considering the fact that natural ventilation occurs rarely and episodically, there have been calls to artificially ventilate the deep basins in order to increase O_2 levels in the deeper water layers (Stigebrandt and Gustafsson, 2007; De Brabandere et al., 2015; Stigebrandt et al., 2015).

Re-oxygenation of the bottom water following an MBI alters the water column and sediment biogeochemistry. Sedimentary rhodochrosite ($MnCO_3$) is typically formed after an MBI when Mn oxides precipitate in the water column (Turnewitsch and Pohl, 2010) and are deposited onto the sediment where they undergo subsequent conversion to $MnCO_3$ (Huckriede and Meischner, 1996; Lenz et al., 2014). Ventilation of the bottom water also is thought to result in the formation of Fe(oxyhydr)oxides (henceforth termed Fe oxides) in the water column (Turnewitsch and Pohl, 2010) and in the surface sediments (Mort et al., 2010). The cycling of P is particularly sensitive to changes in bottom water O_2 concentrations, since Fe oxides, Mn oxides and $MnCO_3$ can all bind dissolved phosphate (HPO_4^{2-}; Mort et al., 2010; Jilbert and Slomp, 2013). Sediment molybdenum (Mo) is an indicator for the presence of H_2S near the sediment-water interface and hence serves as an excellent proxy for the oxidation state of the sediment (Helz et al., 1996; Scott and Lyons, 2012).

Changes in bottom water O_2 concentrations also have an impact on bacterial communities in the Baltic Sea (Steenbergh et al., 2014; Noffke et al., 2016). In particular, bottom water re-oxygenation enhances the activity of sulphur (S)-oxidising bacteria belonging to the family *Beggiatoaceae* (Noffke et al., 2016). These bacteria are chemotrophic species using sulphide as an electron donor and O_2 as an electron acceptor (Teske and Nelson, 2006). Their activity can lead to the development of a suboxic zone, which may contribute to the preservation of Mn oxides and Fe oxides in the surface sediment (Sulu-Gambari et al., 2016b). These bacteria can incorporate P in their cells by taking up pore water HPO_4^{2-}, subsequently storing it as polyphosphate in their vacuoles which may regulate HPO_4^{2-} fluxes at the sediment-water interface. However, when dissolved O_2 reaches low levels (<10 μM), *Beggiatoaceae* may release HPO_4^{2-} into the pore water (Goldhammer et al., 2010; Brock and Schulz-Vogt, 2011; Dale et al., 2013).

Recently, the third largest MBI since 1880 was observed. From December 2014 to January 2015 a total estimated water volume of 320 km^3 entered the Baltic Sea (Mohrholz et al., 2015), followed by a second smaller MBI in November 2015 (Mohrholz et al., 2016). These events re-oxygenated the bottom waters in the Central Baltic Sea (Holtermann et al., 2017; Neumann et al., 2017), which had been euxinic since 2005. The changes in bottom water O_2 concentrations had a direct impact on the nutrient dynamics in the Baltic Sea. Thus, for example, the exposure of the sediments in the deep basin to O_2 rich water was suggested to lead to a 5–33% reduction in the release of P from sediments in the Baltic Proper based on in-situ measured benthic fluxes and water column profiles (Hall et al., 2017; Sommer et al., 2017). In July 2015, an orange surface layer was observed in sediments from the deep basin in the Central Baltic Sea (Rosenberg et al., 2016; Stigebrandt et al., 2017). Based on the visual observations, this layer was suggested to be enriched in Mn oxides and Fe oxides that were formed as a result of the re-oxygenation (Rosenberg et al., 2016). In April 2016, this layer had become thinner, which was suggested to be related to the reductive dissolution of Mn oxides and Fe oxides following a decline in bottom water O_2 concentrations (Stigebrandt et al., 2017). As described above, the details of the sedimentary cycles of Mn, Fe and P following an inflow have so far been deduced from water column sampling, benthic flux measurements, visual observations of the sediment and from chemical sediment data after the re-establishment of euxinic bottom water conditions. As a consequence, the chemical and mineralogical nature of the Mn-, Fe- and P-bearing deposits in the surface sediments formed directly after re-oxygenation remains unknown. The impact of bottom water re-oxygenation on the forms of Mn, Fe and P in

Baltic Sea sediments and their dynamics has not yet been assessed.

In this study, we present pore water and solid phase data for sediment cores retrieved from six sites and water column data along a water depth gradient in the Eastern Gotland Basin. Our samples were collected in June 2016. Additional samples taken in June 2009 prior to the recent inflows were used for comparison. The objective of this study is to assess the impact of the recent MBIs on the cycling of Mn, Fe and P in surface sediments of the Eastern Gotland Basin, using bulk geochemical analyses, synchrotron-based micro X-ray fluorescence (μXRF) and X-ray absorption spectroscopy (XAS). We show that the recent MBIs led to the development of a surface sediment layer enriched in P-bearing rhodochrosite (Mn-carbonate) and Mn(II) phosphates in the deepest parts of the Eastern Gotland Basin, with only a relatively minor role for Fe oxide bound P. We estimate that only ~5% of the water column HPO_4^{2-} removed from the Eastern Gotland basin as a result of re-oxygenation was sequestered in the sediment.

2. MATERIALS AND METHODS

2.1. Study area and sampling

The Eastern Gotland Basin is located in the Central Baltic Sea (Fig. 1a). In June 2016, six sites located along a water depth gradient in the Eastern Gotland Basin were sampled during a research expedition with *R/V Pelagia* (Fig. 1a; Table 1). Sediment cores were retrieved with a multi-corer (Oktopus GmbH, Germany) at each site. Duplicate bottom water samples were taken directly from the overlying water using 20 mL syringes. At each site, one core was sectioned in a nitrogen purged glovebox for sediment and pore water collection (0.5 cm resolution for the first 2 cm; 1 cm resolution for 2–5 cm). For each depth interval a sediment sub-sample was placed in a pre-weighed glass vial for porosity and solid-phase analysis. The glass vials were transferred into nitrogen purged aluminium bags and stored at −20 °C. The remaining sediment for each depth interval was placed in a 50 mL centrifuge tube and subsequently centrifuged at 4500 rpm for 25 min to collect pore water. A second core was subjected to high resolution depth profiling of dissolved O_2, H_2S and pH. At site BY15, located in the deepest part of the basin, a third core was taken for sediment micro analysis (μXRF and XAS).

Water column depth profiles of dissolved O_2 were obtained at five sites (Fig. 1a), using an O_2 sensor (Sea-Bird) attached to a CTD-Rosette. At site BY15, water column samples were collected using an ultra-clean CTD system with 24 ultra-trace metal clean PVDF samplers of 24 L in two rows of 12 samplers mounted onto a rectangular titanium frame (developed and built by the Royal Netherlands Institute for Sea Research (NIOZ), Texel), which was deployed with a Kevlar hydrowire (De Baar et al., 2008; Rijkenberg et al., 2015). All water column samples were retrieved by applying nitrogen pressure at the top of the sampler. Samples for H_2S and HPO_4^{2-} were collected with 20 mL syringes and filtered (0.45 μm Teflon). To avoid loss of H_2S, the aliquot for H_2S analysis was transferred into a N_2 purged 8 mM NaOH solution immediately after filtration. Acid-washed LDPE bottles (Nalgene™) were

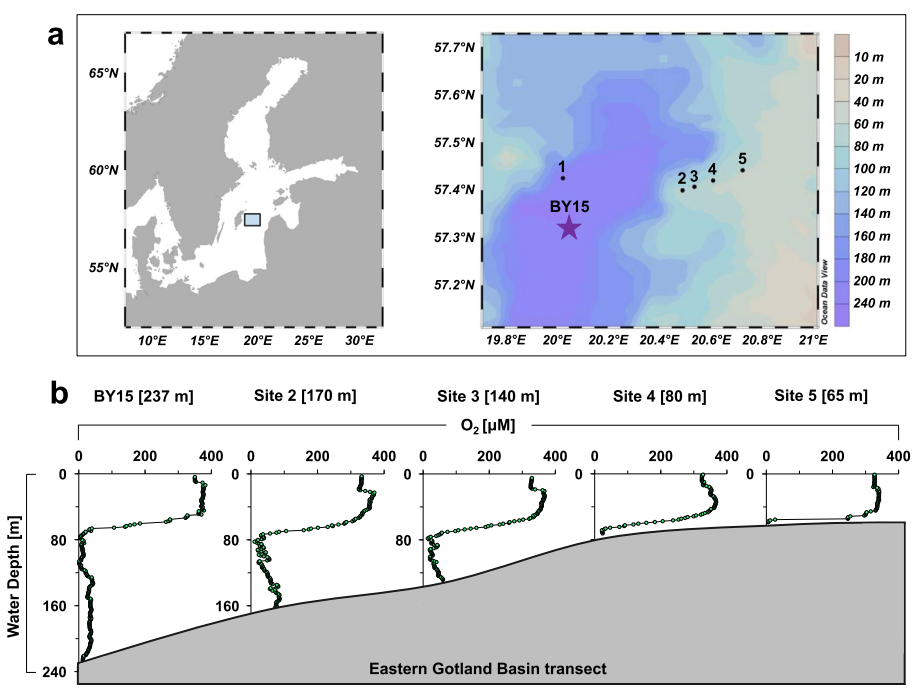

Fig. 1. (a) Map of the Baltic Sea (left) and bathymetric map of the Eastern Gotland Basin showing the locations of the sites presented in this study (right), adapted from Ocean Data View 4 Schlitzer, 2015. The purple star indicates the location of site BY15. Site characteristics are given in Table 1. (b) The green-dotted lines represent water column profiles of dissolved O_2 concentrations for the Eastern Gotland Basin transect. Note that there are no water column data available for site 1 (200 m water depth).

Table 1
Characteristics of the sites sampled in June 2016.

Site	Water depth [m]	Coordinates [N]	Coordinates [E]	Bottom water O_2 [μM]	O_2 penetration depth [mm]	$\sum H_2S$ appearance depth [mm]	S-oxidising bacteria present
BY15	237	57°19.20′	20°3.00′	10	0	0	*Beggiatoaceae*
Site 1	200	57°25.51′	20°1.53′	15	2	6	*Beggiatoaceae and Desulfobulbaceae*
Site 2	170	57°23.98′	20°29.46′	30	3	8	*Beggiatoaceae*
Site 3	140	57°24.42′	20°32.20′	50	1.5	1.5	*Beggiatoaceae*
Site 4	80	57°25.18′	20°36.74′	10	1	1	*Beggiatoaceae*
Site 5	65	57°26.49′	20°43.49′	5	0	2	*Beggiatoaceae*

rinsed three times with the sample collected using acid-washed LDPE tubing connected to the top of the sampler. For the determination of dissolved Mn and Fe, seawater was filtered through a 0.2 μm Sartobran 300 cartridge with a cellulose acetate membrane (Sartorius), pre-rinsed with 0.5 L of seawater. Unfiltered samples for total dissolvable Mn and Fe (henceforth termed total Mn and total Fe) were also collected. Samples for Mn and Fe analyses were acidified to pH 1.8 with distilled HCl and stored at 4 °C until analysis.

Suspended matter samples from the water column at site BY15 were collected through in-situ pumping for 1–4 h at four water depths (85, 175, 200 and 220 m) using four McLane pumps (3× WTS-LV; 1× WTS-LV dual Filter). The water on the filters was removed directly upon retrieval by vacuum pumping and the filters were placed in petri-dishes, sealed in plastic bags and stored at −20 °C until analysis.

Monthly time-series data for dissolved O_2, H_2S and HPO_4^{2-} in the water column at BY15 for January 2002 to September 2018 were obtained from the Swedish Ocean Archive (SHARK) database at the Swedish Meteorological and Hydrological Institute (SMHI; http://sharkweb.smhi.se). Sediment and pore water from a sediment core collected at site BY15 during an expedition with *R/V Aranda* in June 2009 (Jilbert et al., 2011) were analysed for their Mn and P composition, and are assumed to be representative for pre-inflow conditions.

2.2. Water column analyses

Water column samples were analysed colourimetrically for H_2S and HPO_4^{2-} based on methylene and molybdate blue complexes, respectively, using QuAAtro (Bran +Luebbe) gas-segmented continuous flow analysers on board ship (Murphy and Riley, 1962; Grasshoff and Ehrhardt, 1983). Water column Mn concentrations were determined using Inductively Coupled Plasma Mass Spectrometry (ICP-MS; Nexion, Perkin Elmer), after sample preparation using a SC-DX SeaFAST S2 (Elemental Scientific). Acidified samples (pH ~ 2) were pre-concentrated on the SeaFAST system and eluted directly into the ICP-MS and measured online (Lagerström et al., 2013). The blank was 1.012 ± 0.155 nM Mn. Three reference materials were used (NASS-6, SLRS and SLEW) and the overall recovery was 102.4 ± 10.6% (n = 24). Water column Fe concentrations were determined by flow injection using a mixture of luminol and triethylenetetramine with pre-concentration on an iminodiacetic acid resin (Obata et al., 1993; Klunder et al., 2011; Rijkenberg et al., 2014). All Fe in the samples was oxidized to Fe^{3+} by adding 0.1% hydrogen peroxide more than 12 h prior to analysis. The blank of acidified ultrapure water (pH = 1.8) was 25 pM ± 1 pM (n = 30). To ensure the accuracy of the analyses, the system was checked daily using a GEOTRACES standard or an in-house reference material (acidified seawater at pH 1.8). For GEOTRACES SAFe D1, we measured an average value of 0.69 ± 0.26 nM (n = 37) consistent with the community consensus value of 0.67 ← ±0.04 nM (Johnson et al., 2007; www.geotraces.org (2013). Forms of Fe in suspended matter were determined on a quarter of every filter using a 5-step sequential extraction procedure targeting the following phases: (1) ferrihydrite, (2) labile Fe (III) oxides and Fe(II) (iron monosulphide (FeS) + siderite $FeCO_3$), (3) crystalline Fe oxide minerals, (4) magnetite and (5) pyrite (Table 2). Concentrations of Fe were analysed spectrophotometrically (Shimadzu, UV-1800) using the 1–10, phenanthroline method (Cleceri et al., 1998). All extracts, except nitric acid extracts, were passed through a 0.45 μm nylon filter prior to analysis. Concentrations of Mn were measured colourimetrically using a mixed ammonia/formaldoxime reagent, as described in Brewer and Spencer (1971). The sum of all Mn phases extracted in the five Fe extraction steps was assumed to represent reactive Mn (Mn oxides and Mn carbonates; Sulu-Gambari et al., 2016a).

2.3. Pore water collection and analysis

Bottom water and supernatant from each centrifuged sample were filtered through nylon filters (0.45 μm) in a nitrogen purged glovebox for analysis of dissolved pore water constituents. Immediately after retrieval of the pore water, samples for sulphide analyses (0.5 mL) were placed in glass vials filled with a nitrogen purged 8 M NaOH solution (1.5 mL). Samples for HPO_4^{2-} were acidified with 4 μL of 5 M HCl per mL. Concentrations of both H_2S and HPO_4^{2-} were analysed as described for the water column samples. Samples for metals were acidified with 10 μL Suprapur® HCl (35%) per mL and analysed for Mn and

Table 2
Sequential P, S and Fe extractions for suspended matter and sediment samples. The ferrihydrite extraction step from the sequential Fe extraction was only applied to the suspended matter. Unless stated otherwise, all extracts from the sequential extractions were passed through a 0.45 μm nylon filter. The three sequential extraction procedures for P, Fe and S fractionation were performed under strictly anoxic conditions.

Targeted mineral phase	Solvent	Time
SEQUENTIAL PHOSPORUS EXTRACTION[1]		
1 Exchangeable P	1 M $MgCl_2$	0.5 h
2 Easily reducible or reactive ferric Fe-bound P (CDB-P)	Citrate-bicarbonate-CDB buffered to pH 7.5 with Na citrate/Na bicarbonate	8 h
	1 M $MgCl_2$ (wash step)	0.5 h
3 Authigenic P	1 M Na-acetate buffered to pH 4 with acetic acid	6 h
	1 M $MgCl_2$ (wash step)	0.5 h
4 Detrital P	1 M HCl	24 h
5 Organic P	1 M HCl, after ashing at 550 °C	24 h
SEQUENTIAL IRON EXTRACTION[2,3,4]		
1 Ferrihydrite[2]	0.057 M ascorbic acid/0.17 sodium citrate/0.6 sodium bicarbonate	24 h
2 Labile Fe(III) oxides and Fe(II) (iron monosulphide (FeS) + siderite FeCO3)[3]	1 M HCl	4 h
3 Crystalline Fe oxides (goethite, hematite)[3]	0.35 M acetic acid/0.2 M sodium-citrate with 50 g/L sodium dithionite, pH 4.8	4 h
4 Magnetite[4]	0.2 M $(NH_4)_2C_2O_4$/0.17 M $C_2H_2O_4$	6 h
5 Pyrite[3]	HNO_3 (65–70%)	2 h
SEQUENTIAL SULPHUR EXTRACTION[5,6]		
1 Acid-volatile sulphide (AVS)	6 M HCl	24 h
2 Elemental sulphur	Methanol (99.8%)	16 h
Acetone (wash step)		20 min
3 Chromium reducible sulphur (CRS)	500 g/L $Cr(II)Cl_2$ in 32% HCl	48 h

[1] Ruttenberg (1992) as modified by Slomp et al. (1996).
[2] Raiswell et al. (2010).
[3] Claff et al. (2010).
[4] Poulton and Canfield (2005).
[5] Burton et al. (2006).
[6] Burton et al. (2008).

Fe by Inductively Coupled Plasma-Optical Emission Spectroscopy (ICP-OES; Spectro Arcos). Pore water data for Mn and Fe, are assumed to represent Mn^{2+} and Fe^{2+}, although some Mn^{3+} (Madison et al., 2013) or colloidal and nanoparticulate Mn or Fe (Boyd and Ellwood, 2010; Raiswell and Canfield, 2012) might also be present. Concentrations of Mo were determined by ICP-MS (XSeries II, Thermo Fisher Scientific). Samples for NH_4^+ were analysed on board with a QuAAtro (Bran + Luebbe) gas-segmented continuous flow analyser following the phenol-hypochlorite method (Koroleff, 1969). Pore water Mn^{2+} and HPO_4^{2-} in the 2009 samples were determined by ICP-OES as described previously by Jilbert et al. (2011).

2.3.1. High resolution depth profiling

High-resolution depth profiles of pore water O_2 (50-μm), pH (100-μm) and total H_2S (50-μm) were retrieved using microelectrodes and a 2D micromanipulator (Unisense A. S., Denmark) with a step size of 50 to 100 μm. For the O_2 sensor, a 2-point calibration was performed (100% O_2 saturated and N_2 purged artificial seawater) using a calibration chamber (Unisense A.S., Denmark, CAL300). For the calibration of the pH sensor, 3 NBS standards (pH 4, 7 and 10) were used. A TRIS buffer was used to correct for salinity effects (Dickson, 1990; Dickson et al., 2007). The pH is reported on a total scale. For the H_2S sensor calibration, a 5-point calibration was performed with NaS_2 standards. Total H_2S ($\Sigma H_2S = H_2S + HS^- + S^{2-}$) was calculated from the observed H_2S, pH, temperature in Kelvin (T) and salinity (S) (Millero et al., 1988; Jeroschewski et al., 1996).

$$[\Sigma H_2S] = [H_2S] \cdot \left(1 + \frac{10^{-pK_1}}{[H_3O^+]}\right) \quad (1)$$

$$pK_1 = -98.080 + 5765.4/T + 15.0455 \ln(T) + \left(-0.157 \cdot \left(S^{0.5}\right)\right) + 0.0135 \cdot S \quad (2)$$

2.3.2. Diffusive fluxes

Diffusive fluxes of O_2, HPO_4^{2-}, ΣH_2S, NH_4^+ and Mn^{2+} across the sediment-water interface and upward fluxes of ΣH_2S into the suboxic zone were calculated using Fick's first law (Berner, 1980):

$$J = -\phi D_s \cdot \frac{dC}{dz} \quad (3)$$

where J represents the diffusive flux [mmol m^{-2} yr^{-1}], ϕ expresses the sediment porosity, D_s represents the sediment diffusion coefficient [m^{-2} yr^{-1}], C is the concentration of O_2, HPO_4^{2-}, ΣH_2S, NH_4^+ or Mn^{2+} [mM] and z stands for the sediment depth [m]. The diffusion coefficient for the ambient tortuosity, temperature, pressure and salinity at each station was calculated using the R package *marelac* (Soetaert et al., 2010), which implements the constitutive relations listed in Boudreau (1997). For sectioned cores, the concentration gradient at the sediment-water interface was calculated from the difference in concentration in the bottom water and that of in the first sediment depth interval (0–0.5 cm). For micro-electrode profiles, the linear gradient immediately below the sediment-water interface was taken (Malkin et al., 2014). Upward diffusive fluxes of ΣH_2S into the suboxic zone were calculated in a similar manner.

2.4. Solid phase analysis

Surface sediments were analysed on board directly after core collection using a stereomicroscope to assess which S-oxidising bacteria were present at the different sites in the Eastern Gotland Basin. Sediment samples from core slicing were freeze-dried, homogenised and ground to a fine powder with an agate mortar and pestle in an argon purged glovebox. Depth profiles for porosity were derived from the weight loss after freeze-drying, assuming a sediment dry density of 2.65 g cm^{-3} (see Supplementary Information, section 1.1). Sediment weights were corrected for salt content. The amount of salt was calculated from the gravimetric water content and salinity. The freeze-dried samples were stored in air tight jars which were kept in an argon atmosphere at all times to prevent oxidation artefacts (Kraal et al., 2009; Kraal and Slomp, 2014).

2.4.1. Organic carbon content

Aliquots of ~300 mg of freeze-dried sediment were decalcified with 2 wash steps of 1 M HCl as described in Van Santvoort et al. (2002). The samples were subsequently dried at 60 °C, powdered and analysed for carbon using a Fisons Instruments NA 1500 NCS analyser. The organic carbon content was calculated after correction for the weight loss during decalcification. The measurements were normalized to in-house standards, acetanilide, atropine and nicotinamide. Average analytical uncertainty based on duplicate analyses of sediment samples was 0.01 wt. % for organic carbon.

2.4.2. Total manganese, phosphorus and molybdenum contents

For the analysis of the total Mn, P and Mo contents ~100 mg freeze-dried sediment was digested overnight at 90 °C in closed PTFE vessels, using a mixture of HF (40%) and 2.5 mL $HClO_4$-HNO_3 (ratio 3:2). Subsequently, the acid solution was evaporated at 140 °C until a gel was formed. The gel was then dissolved overnight with 1 M HNO_3 at 90 °C. Finally, the Mn, P and Mo concentrations in the 1 M HNO_3 solutions were measured by ICP-OES. To assess the accuracy and precision of the measurements, we used ISE-921 as reference material. The accuracy varied between 97 and 104%, and the relative errors were <4% for all measured elements. The average analytical uncertainty of duplicate samples was 1% for Mn, 1.5% for P and 0.15% for Mo.

2.4.3. Sequential P fractionation

The SEDEX sequential extraction procedure (Ruttenberg, 1992, as modified by Slomp et al., 1996) was applied to determine the sedimentary P phases using ~100 mg of freeze dried sediment. Solid-phase P was fractionated into the following phases (Table 2): (1) exchangeable-P (Ex-P), (2) CDB-P (citrate-bicarbonate buffer), (3) authigenic P (carbonate fluorapatite (CFAP) + biogenic hydroxyapatite + calcium carbonate), (4) detrital P and (5) organic P. Dissolved HPO_4^{2-} in all extracts, except CDB extracts, was analysed colourimetrically on a spectrophotometer (Shimadzu, UV-1800) applying the ammonium heptamolybdate–ascorbic acid method (Strickland and Parsons, 1972). Phosphorus concentrations in the CDB extracts were determined by ICP-OES.

2.4.4. Sequential Fe fractionation

Aliquots of ~80 mg of freeze-dried sediment were used for the Fe solid-phase fractionation using a combination of two extraction methods (Poulton and Canfield, 2005; Claff et al., 2010) as described by Kraal et al. (2017). Solid-phase Fe was fractionated into the following phases (Table 2; step 2–5): (1) labile Fe(III)-oxides and Fe(II) (iron monosulphide $(FeS)^+$ siderite $FeCO_3$), (2) crystalline Fe minerals, (3) magnetite and (4) pyrite (FeS_2). Concentrations of Fe were analysed spectrophotometrically (Shimadzu, UV-1800) using the 1–10, phenanthroline method (Cleceri et al., 1998), except for the Fe in CDB extracts which were analysed by ICP-OES. All extracts were passed through a 0.45 μm nylon filter except for nitric acid extracts.

2.4.5. Sequential S fractionation

Aliquots of ~300 mg freeze-dried sediment were used to determine (1) FeS (Acid Volatile Sulphur, AVS, (2) elemental sulphur and (3) FeS_2 (chromium reducible sulphur, CRS) (Table 2; Burton et al., 2006; Burton et al., 2008). The ZnS concentration formed in the Zn acetate traps was determined by iodometric titration (Cleceri et al., 1998). Elemental sulphur was determined using the cyanide-ferric chloride colorimetric method (Bartlett and Skoog, 1954) and was measured spectrophotometrically (Shimadzu, UV-1800).

2.4.6. Epoxy embedding and desktop μXRF mapping

A vertically intact sub-core from the upper 7 cm of the sediment was taken from a sediment core at site BY15 and embedded with epoxy resin under an argon purged atmosphere for high-resolution elemental mapping (Jilbert et al., 2008; Jilbert and Slomp, 2013; Egger et al., 2015). Subsequently, the epoxy-embedded sub-core was split vertically with a rock saw and polished with alumina powder (0.3 μm). A navigation grid was drilled in the surface of the sub-core, with a micro drill. Exposure time to O_2 was limited to prevent oxidation artefacts (Kraal et al., 2009;

Kraal and Slomp, 2014). High-resolution (30 μm) elemental maps for Mn, Fe, Ca and P were retrieved using a Desktop EDAX Orbis μXRF analyser (Rh tube set at 30 kV, 500 μA, 300 ms dwell-time, equipped with a poly-capillary lens providing a 30 μm spot size).

2.4.7. XAS and synchrotron-based μXRF mapping

Suspended matter samples from the water column and epoxy embedded sediments were examined for their Mn and Fe mineralogy at the European Synchrotron Radation Facility (ESRF) in Grenoble, France, using X-ray Absorption Spectroscopy (XAS). The filters with suspended matter samples were analysed at the Dutch-Belgium beamline (DUBBLE, BM26; Borsboom et al., 1998; Nikitenko et al., 2008). The sediments were analysed at the ID21 beamline (Salomé et al., 2013). At BM26, X-ray Absorption Near Edge Structure (XANES) and Extended X-ray Absorption Fine Structure (EXAFS) spectra were collected on samples in Kapton® tape with an unfocused beam in fluorescence mode using a 9 element Ge detector, and four spectra per sample were merged. Samples were measured within the energy range of 6.50–6.90 keV for Mn and 7.00–7.65 keV for Fe. Levels of Fe in suspended matter were too low to obtain Fe-XANES and Fe-EXAFS spectra of sufficient quality. Therefore, only those for Mn are presented.

At ID21, high-resolution elemental maps of Mn, P, Ca and Fe for epoxy embedded sediment from site BY15 were made. Focusing of the X-ray beam (0.35 × 0.80 μm) was performed by a Kirkpatrick-Baez mirrors system. Identified hotspots of Mn and Fe from the synchrotron-based μXRF maps were further analysed with XANES to determine the mineralogy of Mn and Fe. The XANES spectra were collected within the corresponding energy range, 6.50–6.90 keV for Mn and 7.00–7.65 keV for Fe, respectively. For both measurements, the calibration of the monochromator energy was based on the maximum intensity of the first derivative of Mn foil at 6.53862 keV for Mn and Fe foil at 7.11198 keV for Fe. High-resolution elemental maps were processed using the PyMca X-ray Fluorescence Toolkit (Solé et al., 2007). Subsequently, the ATHENA software package was used to subtract the background and normalise XANES spectra (Ravel and Newville, 2005). Reference standards for hureaulite ($Mn_5^{2+}[PO_3OH]_2[PO_4]_2 \cdot 4H_2O$) and $Mn(III)PO_4$ were obtained from Manceau et al. (2012). Collection of EXAFS spectra at ID21, using a continuously moving monochromator, did not result in spectra of sufficient quality, because of a high noise ratio in the spectra. Therefore, only XANES spectra are presented.

3. RESULTS

3.1. Water column geochemistry

Depth profiles of dissolved O_2 in the water column of the Eastern Gotland Basin, retrieved in June 2016, show saturated levels of O_2 (340–380 μM) in the upper 50 m of the water column (Fig. 1b). From 50 m down to 80 m water depth, the O_2 levels decrease rapidly, reaching a minimum of ~10 μM (Fig. 1b). Below 80 m water depth the concentrations of dissolved O_2 increase, reaching levels up to 50–80 μM, as a result of the deep water renewal (Fig. 1b).

Monthly time-series of dissolved O_2 depth profiles for the time period January 2002 until September 2018 show that the upper 80 m of the water column at site BY15 always contained saturated concentrations of O_2 (Fig. 2a). However, below 80 m water depth, sulphide was generally present, except for two time periods, namely after the MBI that occurred in 2003 and the recent MBIs that took place in December 2014/January 2015 and November 2015. These MBIs consequently led to a removal of all free sulphide in the water column (Fig. 2b) and a two-fold lowering of water column HPO_4^{2-} (Fig. 2c).

The impact of the MBIs on the water column chemistry is further illustrated by the contrasting depth profiles of O_2 and $\sum H_2S$ at BY15 in December 2014 and June 2016 (Fig. 3). While in December 2014, O_2 was only present in the upper part of the water column, in June 2016, O_2 was found below 80 m water depth and reached levels up to ~40 μM (Fig. 3a). At this time, free $\sum H_2S$ was no longer present in the deeper part of the water column (Fig. 3b). The deep water renewal led to a two-fold decrease in water column HPO_4^{2-} (from ~4.6 μM to ~2.5 μM) below 125 m water depth (Fig. 3c).

Concentrations of total Mn in suspended matter in the water column at BY15 increased with water depth from 80 nM (85 m below sea surface; mbss) to 650 nM (220 mbss; Fig. 4a). The concentration of total Fe in suspended matter in the water column showed the opposite pattern, with the highest Fe at 85 m water depth (25 nM; Fig. 4b). Further down in the water column, at 175 m water depth, the concentration of Fe in suspended matter was only 1 nM and below this depth Fe in suspended matter was below the detection limit. Concentrations of total and dissolved Mn were low in surface waters and increased with water depth up to 350 nM and 1840 nM, respectively (Fig. 4c). Total and dissolved Fe concentrations were low in surface waters, reached a maximum between 70 and 85 m, and were low again below 85 m (Fig. 4d).

The normalized Mn-XANES and Mn-EXAFS spectra of the suspended matter from the water column collected at site BY15 (85, 175, 200 and 220 m water depth) are very similar with respect to the positioning of the peaks and post-edge oscillations (Fig. 5). Both the Mn-XANES and Mn-EXAFS spectra of the suspended matter show great similarity with those of birnessite (Fig. 5). The increase in quality of the spectra with water depth reflects the amount of Mn on the filters. In summary, the Mn-XANES and Mn-EXAFS spectra of the water column samples indicate that birnessite is the dominant Mn phase in suspended matter in the water column at site BY15.

3.2. Microscopy and high resolution depth profiles of pH, O_2 and H_2S

Microscopic observations of the surface sediments revealed that *Beggiatoaceae* were present at all sites (Table 1; Supplementary Fig. S1). Another type of S-oxidising bacteria, more commonly known as cable bacteria, belonging to

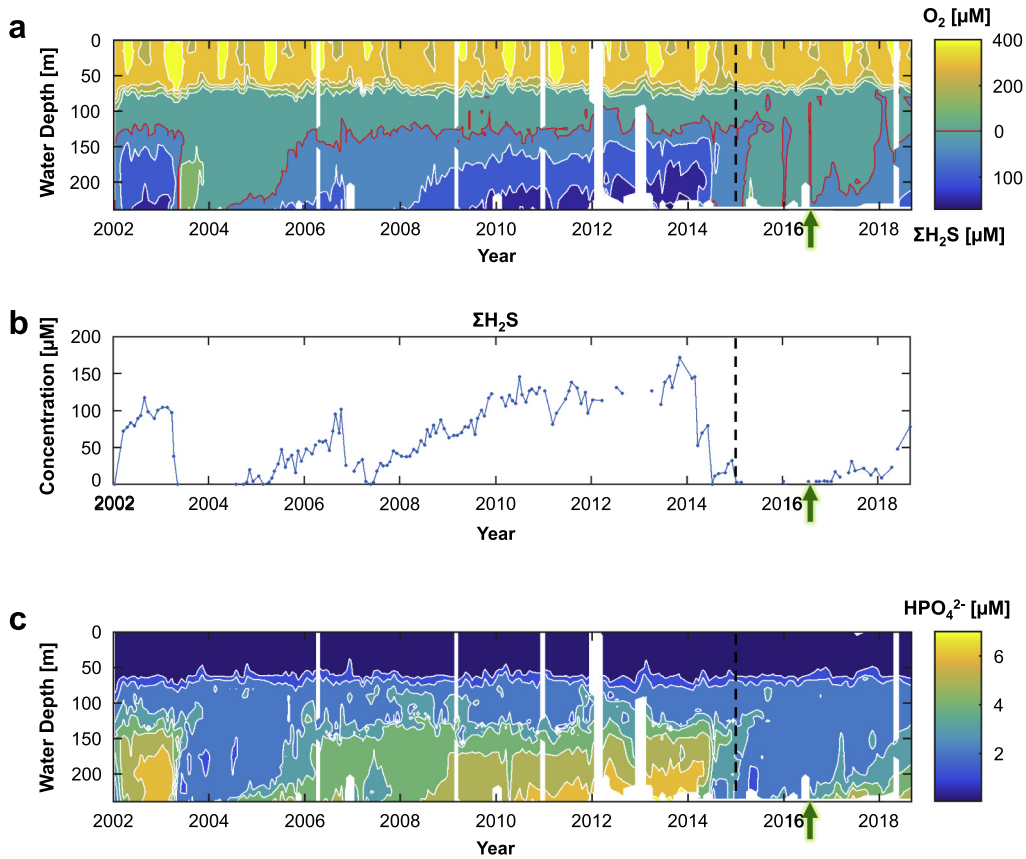

Fig. 2. (a) Time-series of monthly water column depth profiles of dissolved O_2 and ΣH_2S at site BY15 for January 2002 – September 2018. The red line indicates the boundary between O_2 and ΣH_2S (b) Time-series of monthly bottom water ΣH_2S concentrations at 225 m water depth for January 2002 – September 2018. (c) Monthly time-series (January 2002 – September 2018) of dissolved HPO_4^{2-} in the water column at site BY15. The data presented in panel a, b and c were derived from the Swedish Ocean Archive (SHARK) database at the Swedish Meteorological and Hydrological Institute (SMHI; http://sharkweb.smhi.se). The dotted black line in panels a, b and c indicates the time point at which the recent MBIs occurred. The green arrow indicates the time of sampling.

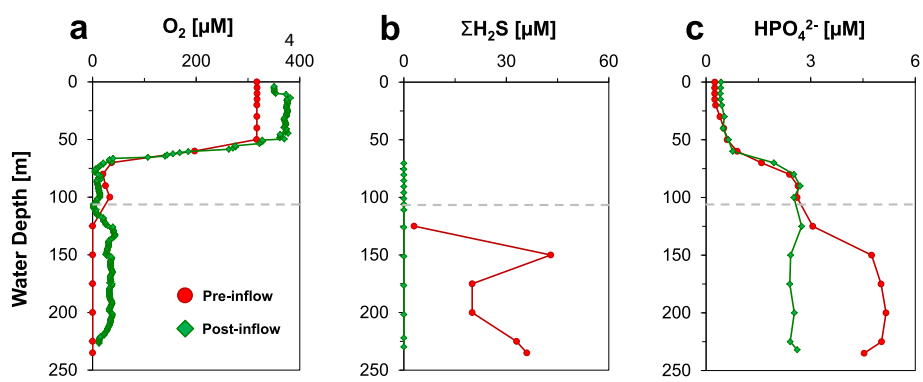

Fig. 3. (a) Comparison of water column O_2 for December 2014 and June 2016. (b) Comparison of water column ΣH_2S for December 2014 (from SHARK database) and June 2016. (c) Comparison of water column HPO_4^{2-} for pre-inflow conditions (averaged over a two year time period covering 2013–2014) and post-inflow (averaged over a 5 month time period covering February 2016 – June 2016). These depth profiles of HPO_4^{2-} were averaged to smooth the trend. The deeper water layer affected by the inflow is below the grey line.

the family *Desulfobulbaceae*, was visually observed at site 1 (Supplementary Fig. S1). Oxygen was present in the bottom water at all sites with concentrations varying from 5 to 50 µM (Fig. 6; Table 1). Bottom water O_2 concentrations were highest at site 2 (30 µM) and 3 (50 µM). The oxygen penetration depth at site 1, 2, 3 and 4 varied from 1 to 3 mm (Fig. 6; Table 1). At BY15 and site 5, O_2 did not penetrate into the sediment (Fig. 6). High resolution depth pro-

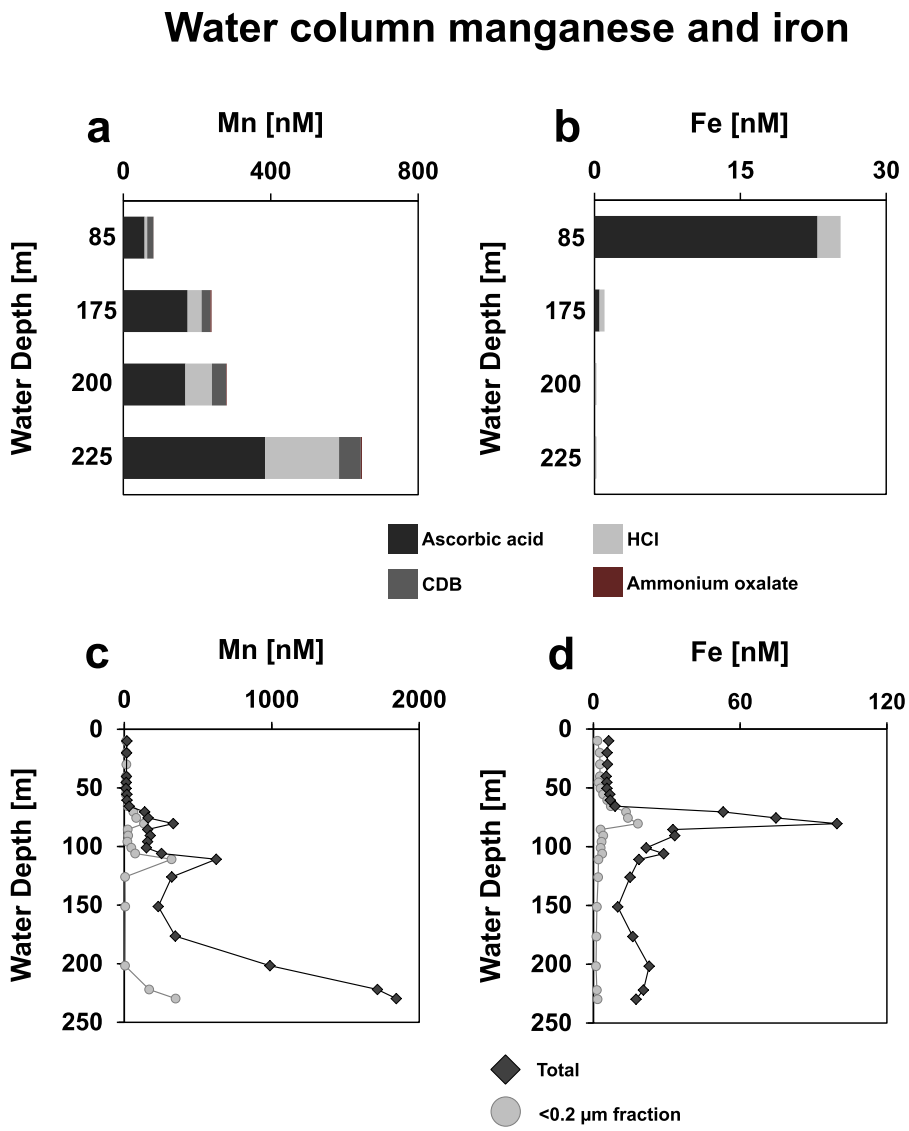

Fig. 4. Water column depth profiles of total Mn (a) and Fe (b) in suspended matter at site BY15 from four water depths in June 2016. Levels of Fe in the CDB and ammonium oxalate step were below the detection limit. Water column depth profiles of total Mn, the Mn < 0.2 µm fraction (c), total Fe and the Fe < 0.2 µm fraction (d) at site BY15 in June 2016. The difference between the Mn and Fe contents in panels c and d is likely related to the difference in detection limit of the methods used.

files show an increase of ΣH_2S in the pore water with depth in the sediment at all sites (Fig. 6). Sulphide was present near the sediment water interface at site BY15. Site 1 and 2 are characterised by a suboxic zone (~4 mm) that lacks both dissolved O_2 and ΣH_2S. At sites BY15, 1 and 2, a pH maximum was observed in the surface sediment, followed by a pH decline with depth in the surface sediment. The strongest pH excursion was found at site 1 where the pH increased by 0.7 units (from pH 8 to 8.7) near the sediment water interface and decreased by 1.2 units (from 8.7 to 7.5) in the upper 5 cm of the sediment. At sites 3, 4 and 5 the pH remained rather constant with depth (Fig. 6). The combination of the pH, O_2 and H_2S profiles at sites BY15, 1 and 2 is typical for an active *Beggiatoaceae* community in surface sediments (Supplementary Fig. S2).

3.3. Pore water profiles

Dissolved Mn^{2+} in the pore water was highest at sites BY15 and 1, reaching values up to 450 µM, while much lower concentrations of 35–80 µM were found at sites 2 and 3 respectively (Fig. 7). At sites 4 and 5, dissolved Mn^{2+} in the pore water was below the detection limit. Dissolved Fe^{2+} was only present in the pore water at site 5 where it reached concentrations up to ~150 µM. Dissolved HPO_4^{2-} generally increased with depth in the sediment at all sites. Only at site BY15, very little HPO_4^{2-} was present in the upper 1.5 cm of the sediment. Dissolved sulphide appeared at ~2 cm depth at sites BY15, 1 and 2 reaching concentrations up to ~360 µM. These three sites are thus characterized by a sub-oxic zone. Sites 3 and 4 contained

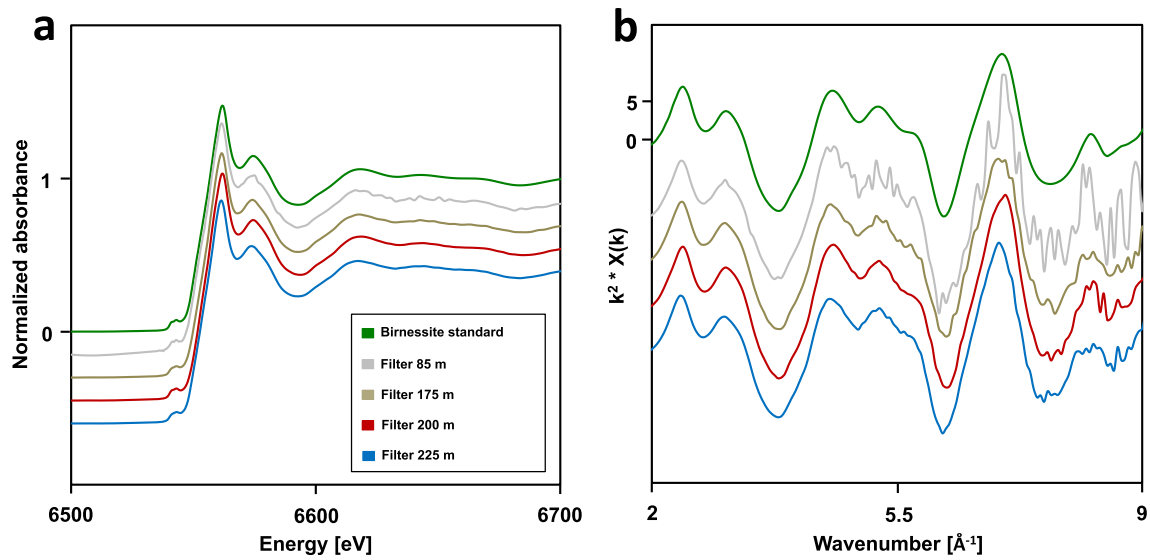

Fig. 5. (a) Normalized manganese XANES spectra of birnessite and suspended matter in the water column collected at 85, 175, 200 and 225 m water depth at site BY15. (b) Manganese k^2 weighed EXAFS spectra of birnessite and suspended matter in the water column at the same water depths.

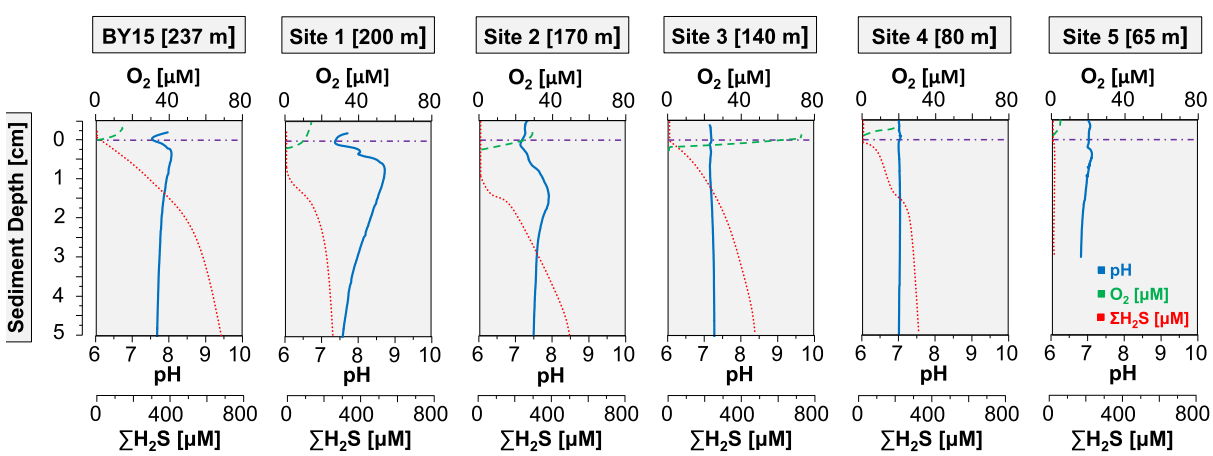

Fig. 6. High resolution pore water depth profiles of dissolved O_2 (green-dashed line), ΣH_2S (red-dotted line) and pH (blue line) for six sites along the Eastern Gotland Basin depth transect (June 2016). The pH is reported on a total scale and corrected for salinity effects. The dashed-dotted purple line represents the sediment water interface. The oxygen penetration depth and sulphide appearance depth are reported in Table 1. (For interpretation of the references to colour in this figure legend, the reader is referred to the web version of this article.)

sulphide throughout the entire depth of the sediment. The shallowest site 5 had low background concentrations of ΣH_2S (<9 µM). Dissolved NH_4^+ levels increased with depth in the sediment at all sites reaching concentrations up to ~150 µM. Our results are indicative of the release of Mo into the pore water at BY15 and site 1. A comparison of pore water profiles of Mn^{2+} and HPO_4^{2-} for 2009 and 2016 (pre- and post-inflow, respectively) at site BY15, suggests that the oxygenation of the bottom water led to an increase in dissolved Mn^{2+} and a decrease in HPO_4^{2-} in the upper 5 cm of the sediment (Fig. 8).

3.4. Diffusive fluxes

The estimated uptake of O_2 by the sediment ranged from 0.11 to 4.90 mmol m^{-2} d^{-1} (Table 3). The estimated benthic release of H_2S ranged from 1.13 to 4.17 mmol m^{-2} d^{-1}. Upward diffusive fluxes of H_2S into the suboxic zone ranged from 0.12 to 2.02 mmol m^{-2} d^{-1}. The higher H_2S fluxes derived from the micro electrodes in comparison to the H_2S fluxes calculated from pore water concentrations from core sectioning can be explained by sulphide loss during core slicing. Benthic release of HPO_4^{2-} ranged from 0.01 to

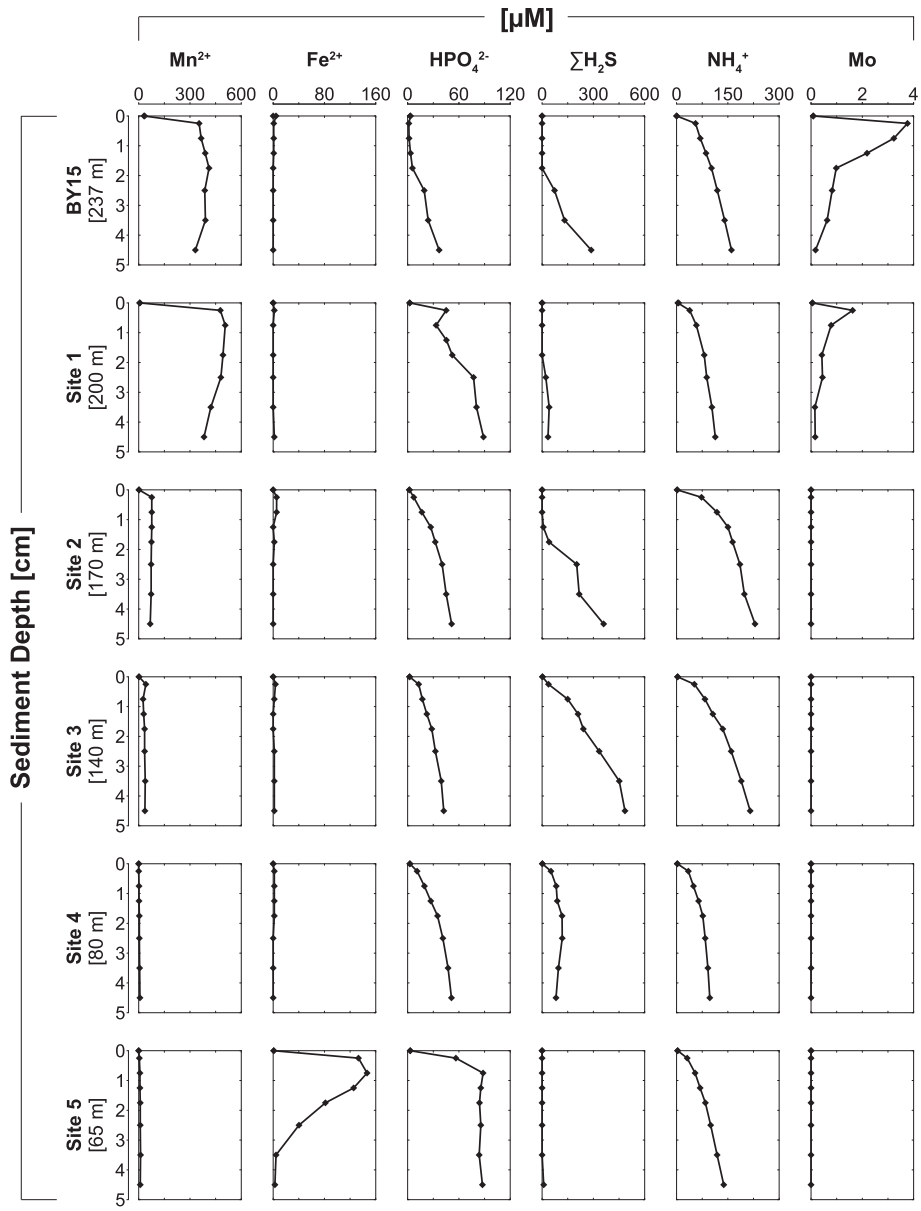

Fig. 7. Pore water depth profiles of dissolved Mn^{2+}, Fe^{2+}, HPO_4^{2-}, ΣH_2S, NH_4^+ and Mo for the upper 5 cm of the sediment at sites BY15 and 1 to 5 (June 2016).

0.27 mmol m^{-2} d^{-1}, whereas benthic NH_4^+ fluxes ranged from 0.89 to 2.76 mmol m^{-2} d^{-1}. Benthic fluxes of Mn^{2+} were highest at site BY15, 1 and 2 and decreased with water depth, ranging from 6.5 mmol m^{-2} d^{-1} at site 1 down to 0 mmol m^{-2} d^{-1} at site 5. A comparison of the sediment-water exchange rates of HPO_4^{2-}, NH_4^+ and Mn^{2+} for 2009 and 2016 at site BY15 (pre- and post-inflow, respectively), suggest a decline in the benthic release of HPO_4^{2-} (from 0.04 to 0.01 mmol m^{-2} d^{-1}) but an increase in that of NH_4^+ (from 0.5 to 2.2 mmol m^{-2} d^{-1}) and Mn^{2+} (from 0.1 to 4.4 mmol m^{-2} d^{-1}) due to the re-oxygenation.

3.5. Solid-phase profiles

Strong enrichments in total Mn were observed near the sediment-water interface at sites BY15 (~1000 µmol g^{-1}) and site 1 (~2500 µmol g^{-1}), but very little Mn was present in the sediment at depth at these sites and throughout the profiles at the other four sites (Fig. 9). Sites BY15 and 1 are also characterized by enrichments in labile Fe(III) oxides near the sediment–water interface (~45 and ~115 µmol g^{-1}, respectively; Fig. 9). In contrast, sites 2, 3, 4 and 5 do not show such an enrichment and are largely

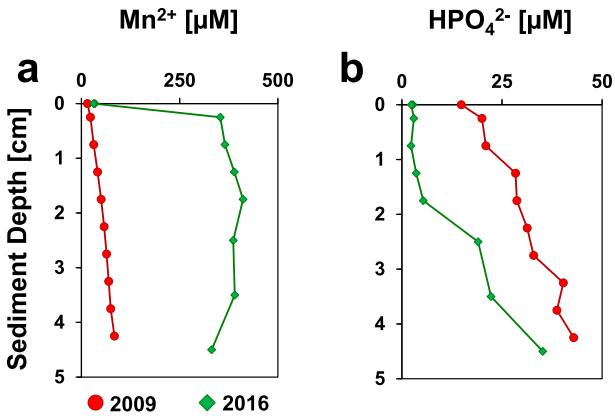

Fig. 8. Comparison of pore water Mn^{2+} (a) and HPO_4^{2-} (b) at site BY15 for 2009 and 2016 (pre-inflow and post-inflow, respectively).

devoid of labile Fe(III) oxides. Concentrations of iron monosulphide were low at site BY15, 1 and 4, highest at site 2 and 3 and below the detection limit at site 5 (Fig. 9). Pyrite concentrations mostly increased with depth in the sediment (Fig. 9). Sediments at site 4 and 5 were relatively low in pyrite (~70 µmol g^{-1}). Sediment molybdenum was highest (~3 µmol g^{-1}) at the deepest site (BY15) and decreased with decreasing water depth along the transect (Fig. 9).

We observed substantial enrichments in Ex-P and CDB-P at the deepest sites in the Eastern Gotland Basin (BY15; ~50 µmol g^{-1}, site 1; ~120 µmol g^{-1}; Fig. 10). Levels of authigenic and detrital P in the surface sediments remained relatively constant with depth at all sites. Organic-P decreased with decreasing water depth along the transect (Fig. 10). Bottom water re-oxygenation led to an increase in total Mn, Ex-P^+ CDB-P and total P in the upper 2 cm of the sediment at site BY15 as revealed by the change in concentration between 2009 (pre-inflow) and 2016 (post-inflow) (Fig. 11; Table 4). The increase in total P following the inflow led to a decrease in the C_{org}/total P ratio in the surface sediment (Fig. 11d).

3.6. XANES, EXAFS and high-resolution elemental mapping of surface sediment

Desktop µXRF mapping of Mn, P, Ca and Fe using epoxy embedded surface sediment (upper 10 mm), revealed that the spatial distribution of Mn at BY15 closely resembled that of P and Ca (Fig. 12). A well-defined layer strongly enriched in Mn, P and Ca was observed in the upper 1.5 mm of the surface sediment of BY15, whereas a background in sedimentary Fe was found below 1.5 mm. A secondary layer concentrated in Mn, P and Ca was observed at 3 mm depth.

The normalized Mn XANES spectra collected at Mn-rich spots 1 to 5, in the upper 0.6 mm of the surface sediment, were very similar to the spectrum of rhodochrosite (Figs. 13a and 14a). The Mn-XANES spectra in the interval between 4.6 and 4.8 mm were distinctly different from those

Table 3
Calculated diffusive fluxes of O_2, ΣH_2S, HPO_4^{2-}, NH_4^+ and Mn^{2+} at the sediment-water interface (unless indicated otherwise) for pre-inflow (2009; BY15 only) and post-inflow (2016) conditions. Note, that only the sites below 80 m water depth were subjected to bottom water re-oxygenation. The O_2 fluxes and the ΣH_2S fluxes highlighted with a blue rectangle were calculated based on high resolution depth profiles obtained with micro electrodes, whereas all the other fluxes were calculated based on pore water profiles from core sectioning. Upward diffusive fluxes of ΣH_2S into the suboxic zone are highlighted in bold and underlined. N/A: not available. Negative and positive values indicate a downward and upward flux, respectively. *Data from Jilbert et al. (2011).

Site	Water depth [m]	O_2 [mmol m^{-2} d^{-1}]	ΣH_2S [mmol m^{-2} d^{-1}][1]	ΣH_2S [mmol m^{-2} d^{-1}][2]	HPO_4^{2-} [mmol m^{-2} d^{-1}]	NH_4^+ [mmol m^{-2} d^{-1}]	Mn^{2+} [mmol m^2 d^{-1}]
BY15 (pre-inflow)	237	-	N/A	N/A	0.04	0.54*	0.10
BY15	237	-1.01	4.17	**0.93**	0.01	2.22	4.44
Site 1	200	-0.54	**1.38**	**0.21**	0.5	1.35	6.52
Site 2	170	-1.12	**2.02**	**0.57**	0.06	2.76	1.00
Site 3	140	-4.90	2.00	1.13	0.11	1.79	0.50
Site 4	80	-0.71	3.21	1.47	0.08	1.07	0.00
Site 5	65	-0.11	**0.12**	**0.07**	0.27	0.89	0.02

[1]Microprofiles.
[2]Core sectioning.

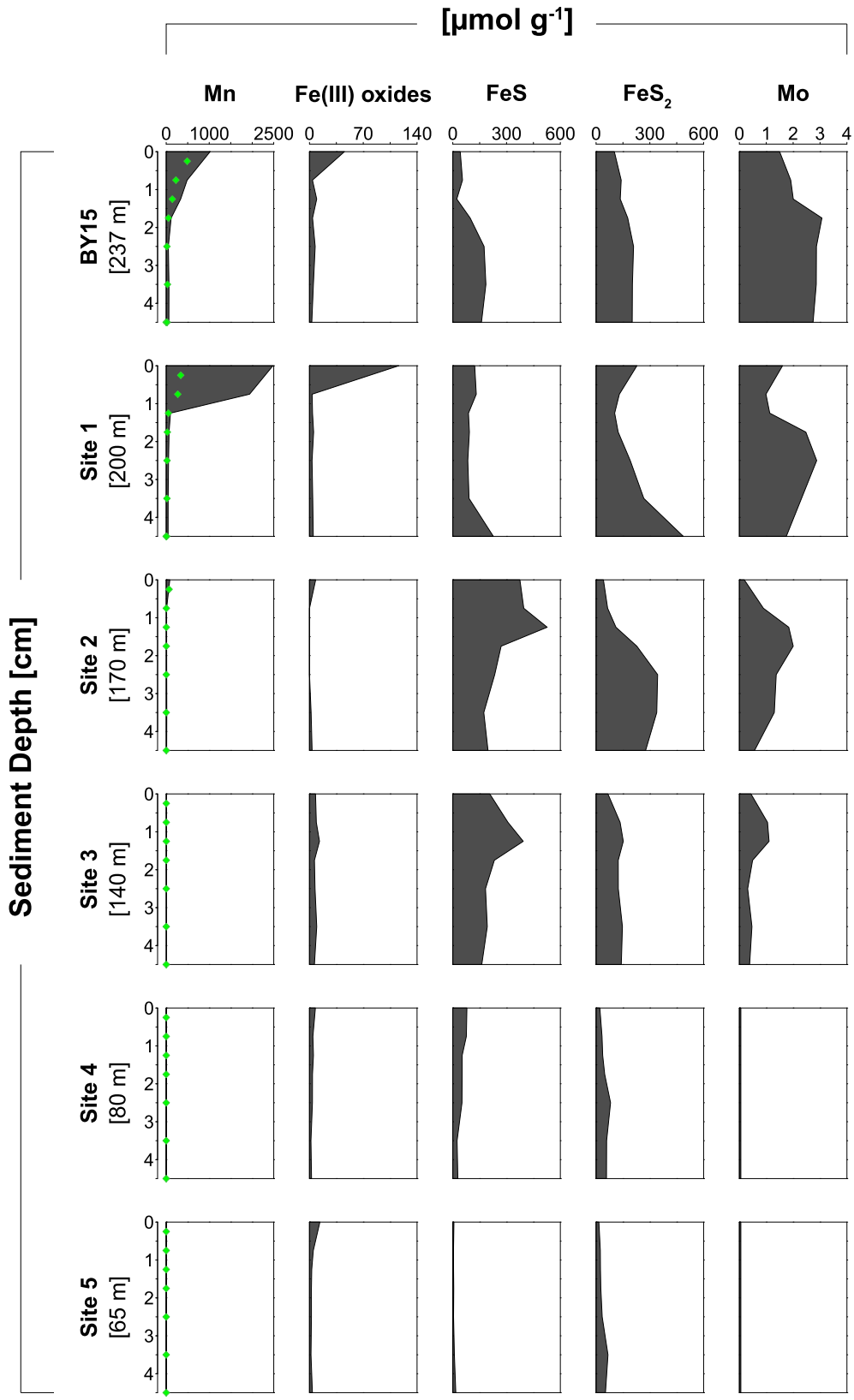

Fig. 9. Depth profiles of sediment Mn, labile Fe(III) oxides, Fe monosulphide (FeS), pyrite (FeS_2) and molybdenum (Mo). The green diamonds represent the Mn extracted in the CDB step of the SEDEX procedure. (For interpretation of the references to colour in this figure legend, the reader is referred to the web version of this article.)

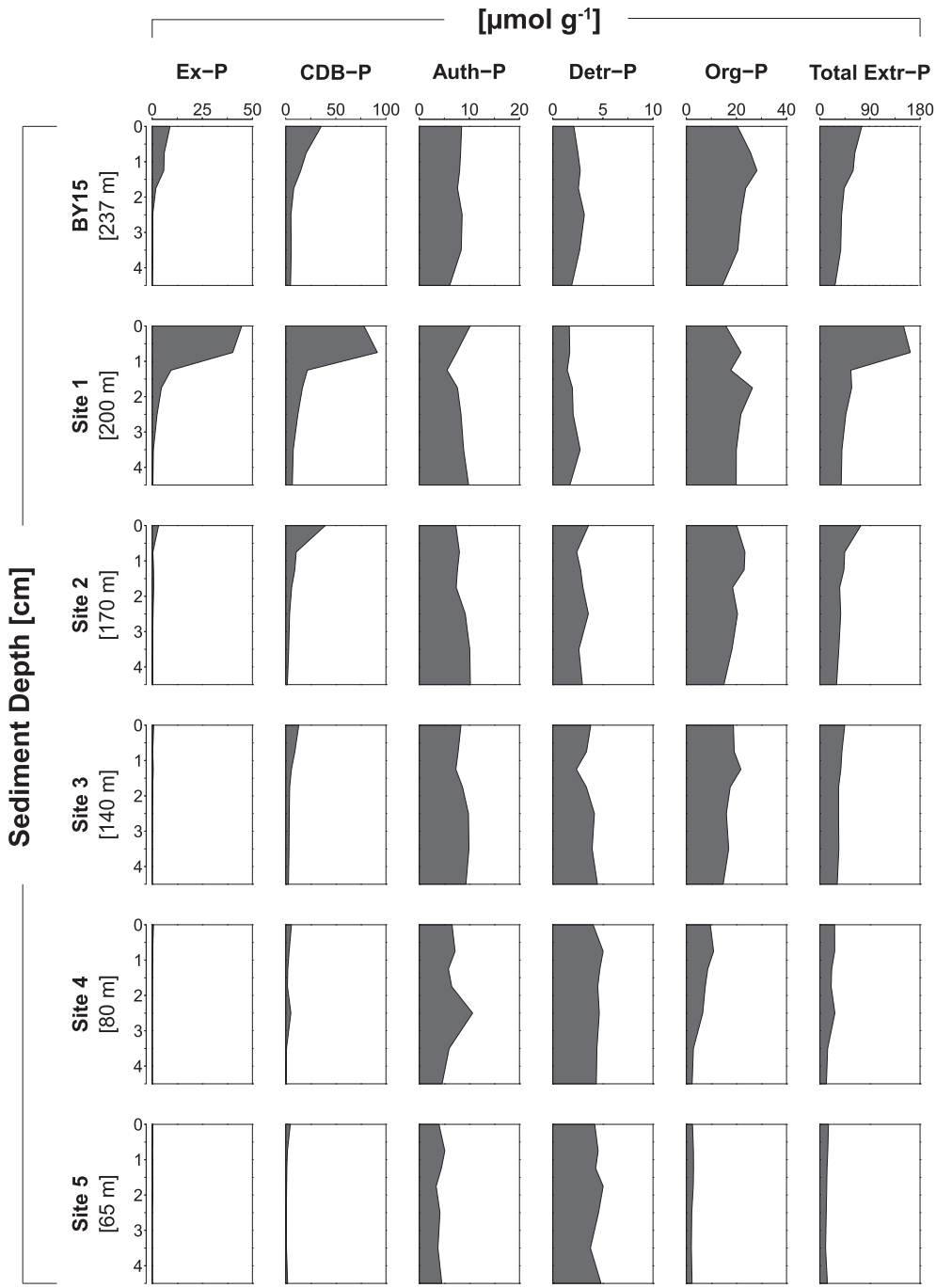

Fig. 10. Sedimentary phosphorus speciation (Ex-P, CDB-P, Auth-P, Detr-P, Org-P and Total Extr-P) for the upper 5 cm of the sediment at sites BY15 and 1 to 5 (June, 2016).

collected in the upper 0.6 mm of the sediment. Spectra collected in Mn-rich spots 7–11 resemble those of hureaulite, a Mn(II) phosphate (Figs. 13.b and 14a). The spectrum collected at spot 6 (Fig. 13b) is a hybrid signal that can be reproduced by linear combination fitting of the XANES spectra of rhodochrosite and hureaulite (Fig. 14a; Supplementary Fig. S4). In this part of the sediment Mn, P and Ca are strongly correlated (Supplementary Fig. S3a and b).

Deeper in the sediment in the interval from 7.5 to 7.9 mm, the enrichment of Mn was less pronounced (Fig. 13c). Relative enrichments in Mn in this depth interval coincided with high Fe and S contents. The Fe and S in these enrichments showed a strong correlation with Mn (Supplementary Fig. S3c). The shape of the Mn XANES spectra resembled that of Fe in pyrite, which has been collected at the Fe K edge, suggesting that in this part of the

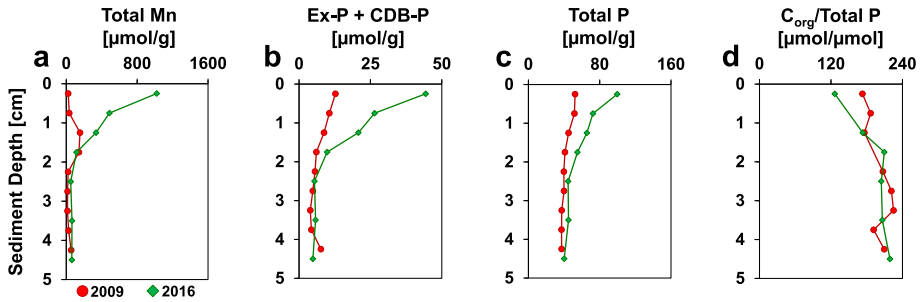

Fig. 11. Depth profiles of (a) total Mn, (b) Ex-P + CDB-P, (c) total P and (d) C_{org}/total P ratio at site BY15 in 2009 (red; pre-inflow) and 2016 (green; post-inflow). (For interpretation of the references to colour in this figure legend, the reader is referred to the web version of this article.)

Table 4
Comparison of sediment P speciation at site BY15 for pre-inflow (2009) and post-inflow conditions (2016).

	Sediment depth	Ex-P [µmol/g]	CDB-P [µmol/g]	Ca-P [µmol/g]	Detr-P [µmol/g]	Org-P [µmol/g]	Total-P [µmol/g]
BY15 (2016)							
0–0.5	cm	8.89	35.46	8.46	2.10	20.40	99.66
0.5–1	cm	6.02	20.44	8.25	2.51	25.66	72.42
1–1.5	cm	5.80	15.00	8.06	2.74	28.18	65.61
1.5–2	cm	1.83	8.02	7.64	2.56	23.68	55.04
2–3	cm	0.22	5.18	8.56	3.15	21.89	44.55
3–4	cm	0.26	5.53	8.37	2.69	20.56	44.99
4–5	cm	0.06	4.79	6.07	1.88	14.43	40.19
BY15 (2009)							
0–0.5	cm	1.97	10.78	4.47	0.81	13.35	52.37
0.5–1	cm	1.94	8.68	5.28	0.75	13.51	51.64
1–1.5	cm	1.14	7.60	6.36	1.01	12.75	45.09
1.5–2	cm	0.06	6.01	6.89	1.13	14.54	41.00
2–2.5	cm	0.16	5.42	7.06	1.08	15.52	39.76
2.5–3	cm	0.41	4.42	6.30	0.84	12.92	39.98
3–3.5	cm	0.42	3.52	7.31	1.14	15.27	37.40
3.5–4	cm	0.12	4.20	6.48	1.15	N.A.	37.17
4–4.5	cm	0.19	7.46	5.64	1.08	13.06	37.30

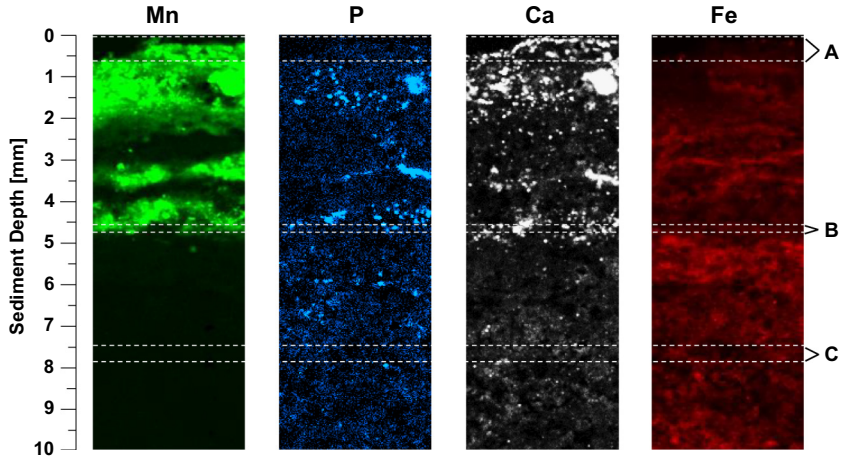

Fig. 12. Desktop µXRF maps of Mn (green), P (blue), Ca (grey) and Fe (red) in the top 10 mm of epoxy-embedded sediment at BY15. These maps are shown in true vertical orientation and the brightness was adjusted to emphasize the features in the sediment. Zone A (0–0.6 mm), B (4.6–4.8 mm) and C (7.5–7.9 mm) represent the sediment depth intervals that were mapped at ID21 at the ESRF in Grenoble (Fig. 13). (For interpretation of the references to colour in this figure legend, the reader is referred to the web version of this article.)

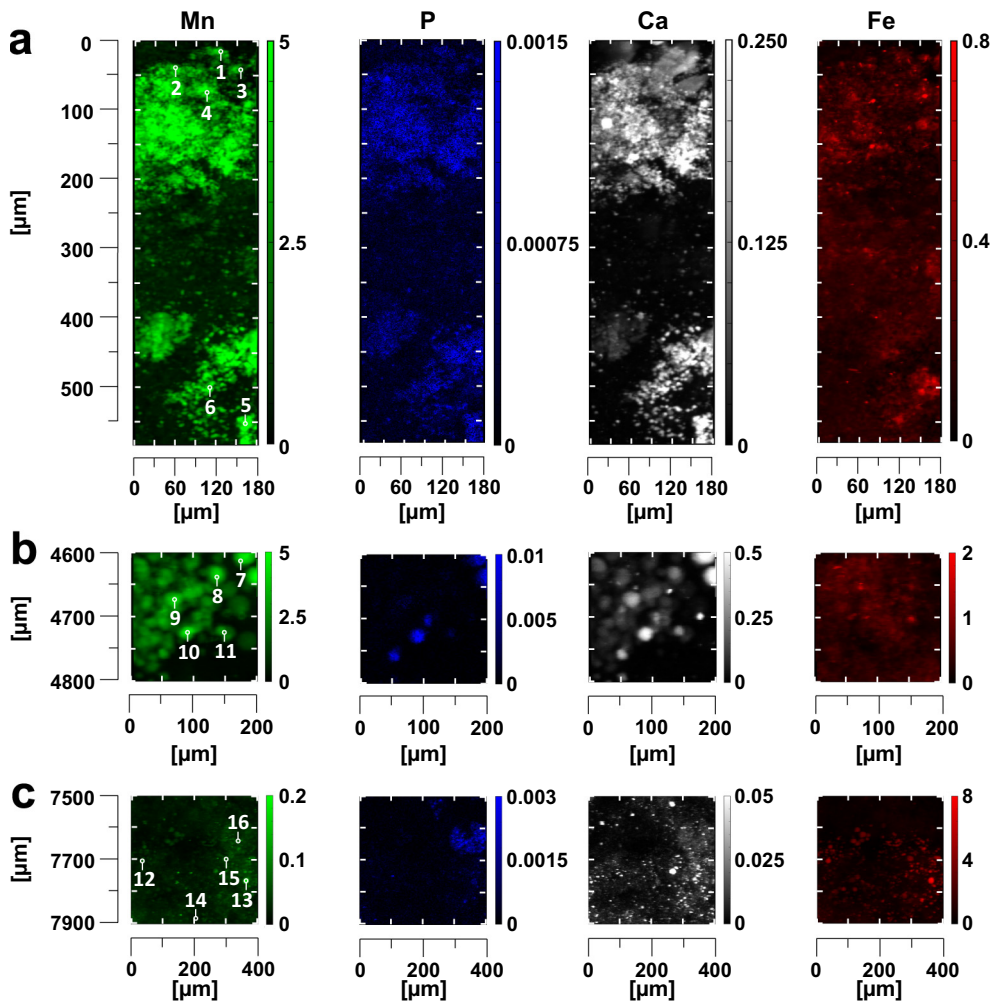

Fig. 13. Synchrotron-based high-resolution (1 µm) µXRF maps of Mn (green), P (blue), Ca (white) and Fe (red) for the top 8 mm of epoxy-embedded sediment at BY15. These maps are shown in true vertical orientation The colours accentuate relative count intensities that are adjusted for brightness and contrast to emphasise the features in the sediment. These maps were created using the PyMca X-ray Fluorescence Toolkit (Solé et al., 2007). The white labels with corresponding numbers indicate the spots for which Mn XANES spectra were collected (Fig. 14). (a) Elemental µXRF maps of the 0–0.6 mm sediment depth interval. (b) Elemental µXRF maps of the 4.6–4.8 mm sediment depth interval. (c) Elemental µXRF maps of the 7.5–7.9 mm sediment depth interval. (For interpretation of the references to colour in this figure legend, the reader is referred to the web version of this article.)

sediment Mn is associated with pyrite (Fig. 14b). A comparison of the available part of the Mn EXAFS spectrum to that of Fe in pyrite supports this interpretation (Supplementary Fig. S5). Other Mn XANES spectra collected at spots which did not show significant enrichments in Mn, Fe, P or S represented a fourth type of Mn in the surface sediment (Fig. 14b). The position of the edge and the shape of the XANES spectrum was similar to the spectrum interpreted as background Si-bound Mn in Lenz et al. (2014).

4. DISCUSSION

4.1. Impact of re-oxygenation on water column chemistry

During MBIs, saline and oxygenated North Sea water mixes with and partly replaces the euxinic deep waters in the Eastern Gotland Basin (Schneider, 2011). As a consequence, nutrient and H_2S-rich waters from the deep basin are pushed upward in the water column and transferred laterally to the north and east while becoming distributed over a larger surface area (Reissmann et al., 2009; Eilola et al., 2014). Changes in water column chemistry are thus the compound result of re-oxygenation and replacement of the deep water.

Our results highlight that the deep water renewal in 2014 and 2015 indeed led to an increase in O_2 and complete removal of $\sum H_2S$ below 125 m water depth (Fig. 2). Research on previous MBIs has shown that increased O_2 concentrations in the water column always led to major changes in its Mn, Fe and P chemistry (Turnewitsch and Pohl, 2010). Prior to these MBIs, concentrations of dissolved Mn^{2+} and Fe^{2+} typically ranged from 5 to 15 µM and 1 to 1.5 µM (Dellwig et al., 2010; Turnewitsch and Pohl, 2010; Dellwig et al., 2018), while particulate Mn

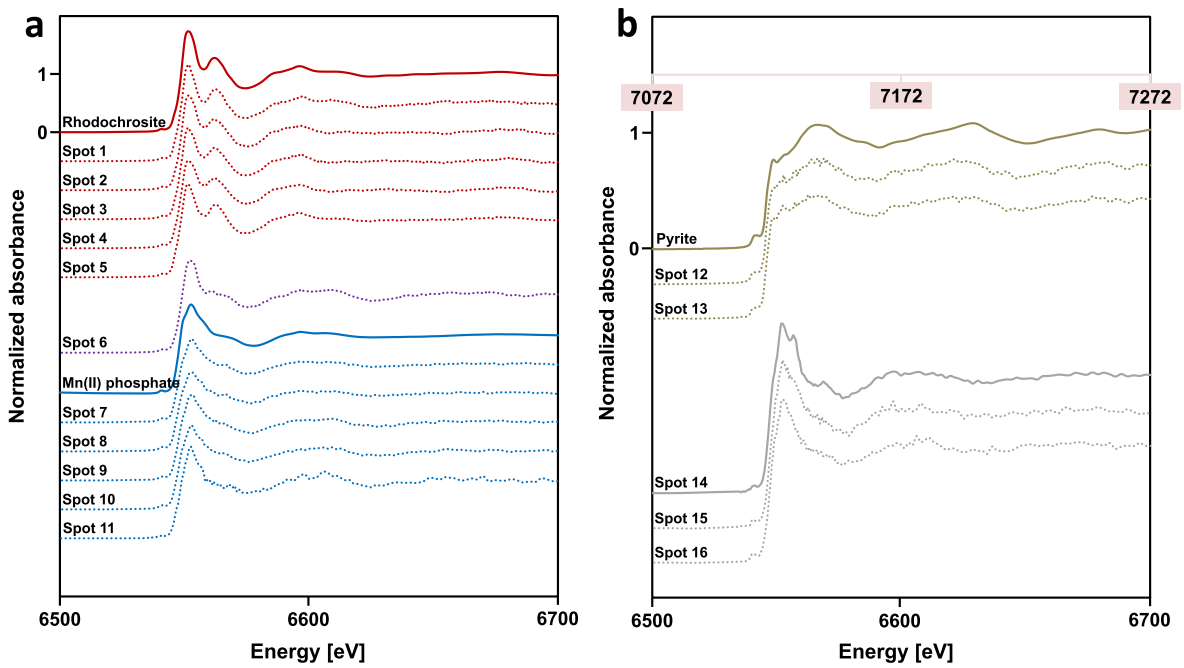

Fig. 14. (a) Normalised Mn XANES spectra of the surface sediment at site BY15. XANES spectra from spots 1 to 5 (red) resemble the spectrum of rhodochrosite. XANES spectra from spot 7 to 11 (blue) are similar to the spectrum of Mn(II) phosphate. The spectrum from spot 6 contains features of the XANES spectra of both, rhodochrosite and Mn(II) phosphate. (b) Normalised Mn XANES spectra of the subsurface sediment at site BY15. The Mn spectra from spots 12 and 13 (gold) have a similar shape as the XANES spectrum of Fe in pyrite. XANES spectra from spots 14 to 16 (grey) show features that are similar to the XANES spectrum that was interpreted as background Si-bound Mn in Lenz et al. (2014). (For interpretation of the references to colour in this figure legend, the reader is referred to the web version of this article.)

and Fe concentrations generally were at least an order of magnitude lower (Turnewitsch and Pohl, 2010). Previous MBIs led to the removal of most of the dissolved Mn^{2+} and Fe^{2+} and formation of Mn oxides and Fe oxides in the water column (Huckriede and Meischner, 1996; Turnewitsch and Pohl, 2010; Yakushev et al., 2011; Pohl and Fernández-Otero, 2012).

In June 2016, approximately 7 months after the 2015 inflow, particulate Mn, which we show was in the form of the Mn oxide birnessite (Fig. 5), was still present in the lower part of the water column at concentrations ranging up to ~1800 nM (Fig. 4). Almost no Fe^{2+} was present in the water column. The concentrations of Fe oxides and total Fe in the suspended matter in the water column (<70 nM) (Fig. 4b and d) were much lower than those for Mn. The contrasting behaviour of Mn and Fe in the water column is the direct result of the less efficient sequestration of Mn in mineral form in the sediment under permanently anoxic conditions and the slower oxidation kinetics of Mn^{2+} with O_2 when compared to Fe^{2+} (Burdige, 1993). Furthermore, FeS formation upon contact of Fe^{2+} with sulphide prevents escape of Fe^{2+} from the sediment into the water column. As a consequence, an order of magnitude higher Mn^{2+} concentrations than those of Fe^{2+} build-up in the anoxic water column between MBIs, allowing more Mn oxides to be formed following an inflow. The relatively high abundance of Mn oxide in the lower water column at site BY15 (Fig. 4a and c) is likely due to 'Mn-refluxing', i.e. remobilization of Mn^{2+} from sediment pore water (Fig. 7), formation of Mn oxides in the water column and redeposition of the Mn oxides (Adelson et al., 2001; Sulu-Gambari et al., 2017). To our knowledge, this is the first time that pore water and sediment depth profiles are combined with water column records for the Baltic Sea to show evidence for such Mn-refluxing after an inflow.

We observed a strong decrease in water column HPO_4^{2-} following the most recent MBIs (Figs. 2c and 3c). Based on analysis of water column profiles, various authors have concluded that most of the decrease in water column HPO_4^{2-} below 125 m water depth following MBIs is due to replacement of the HPO_4^{2-} rich, anoxic water by HPO_4^{2-} poor, oxic water originating from the North Sea (Schneider, 2011; Eilola et al., 2014; Almroth-Rosell et al., 2015). Both Mn oxides and Fe oxides are known to act as a carrier of P to the sediment (Dellwig et al., 2010). This implies that re-oxygenation could lead to an enhanced depositional flux of Mn oxides and Fe oxide associated P to the sediment, thus potentially contributing to part of the observed removal of water column HPO_4^{2-}. The role of the depositional flux of metal oxides in removing P from the water column is best assessed by analyzing the oxygenation state (Section 4.2) and chemical composition (Section 4.3) of the sediments.

4.2. Impact of re-oxygenation on O_2 penetration in the sediment and the role of S-oxidising bacteria

The exposure of surface sediments to O_2 rich water, as a result of bottom water ventilation, led to an O_2 penetration into the sediment of up to 3 mm (Fig. 6; Table 1). The

presence of O_2 also induced the activity of S-oxidising bacteria belonging to the family *Beggiatoaceae* (Table 1). The activity of *Beggiatoaceae* is characterized by a distinct biogeochemical signature (Supplementary Fig. S2) with a low pH near the sediment surface due to proton formation and a high pH in the deeper sediment due to proton consumption by sulphide oxidation (Seitaj et al., 2015). The pH gradients in the pore waters of sites BY15, 1 and 2, are indicative of a highly active *Beggiatoaceae* community. Prior to the 2014/2015 MBIs, these *Beggiatoaceae* were only observed in the hypoxic transition zone at 80–120 m water depth (Noffke et al., 2016). In our study, we found active *Beggiatoaceae* mats down to a water depth of 237 m, which is the result of the availability of O_2 in the bottom waters (Table 1; Supplementary Fig. S1a). Another recent study also observed that the activity of *Beggiatoaceae* extended to the deepest part of the Eastern Gotland Basin, as a consequence of bottom water renewal (Sommer et al., 2017).

Microbial mats of *Beggiatoaceae* contribute to the benthic filter for sulphide in the Baltic Sea by linking the oxidation of dissolved H_2S to the reduction of O_2. This is complemented by chemical oxidation of H_2S by Fe oxides and Mn oxides, where they are present in the surface sediment. The resulting suboxic zone (Supplementary Fig. S2) prevents the direct release of sulphide from sediments to the water column (Seitaj et al., 2015; Yücel et al., 2017). We found that the suboxic zone only developed in the surface sediments at site BY15, 1 and 2 (Figs. 6 and 7). The observed differences between the depth profiles of ΣH_2S obtained with micro-electrodes and after pore water sectioning at BY15 are attributed to spatial variability and could be due to spatial differences in the abundance and activity of *Beggiatoaceae*.

Besides their role in oxidation of dissolved H_2S, *Beggiatoaceae* are also capable of taking up pore water HPO_4^{2-} and subsequently storing it as polyphosphate in their vacuoles (Goldhammer et al., 2010; Brock and Schulz-Vogt, 2011; Dale et al., 2013). This mechanism might explain part of the removal of pore water HPO_4^{2-} in the surface sediment at the deepest sites (Figs. 7 and 8b).

4.3. Impact of re-oxygenation on the sediment geochemistry

Sediment records for the Gotland Deep show that deep water re-oxygenation events can lead to the formation of layers of Ca-rhodochrosite from Mn oxides (Heiser et al., 2001; Lenz et al., 2015). We show that the deposition of Mn oxides related to the MBIs indeed resulted in enrichments in Mn in the surface sediment at site BY15 ($\sim$1000 μmol g^{-1}) and site 1 ($\sim$2500 μmol g^{-1}), as revealed by the change in Mn concentration between 2009 (pre-inflow) and 2016 (post-inflow; Fig. 11a). The water depth dependence of the Mn enrichment is likely the combined effect of a greater overlying Mn-bearing water mass at deeper sites and a larger role for gravitational focussing of suspended material (Sulu-Gambari et al., 2017).

We found no evidence for the presence of birnessite in the surface sediment in the resin-embedded core at site BY15, despite the fact that birnessite is the dominant Mn phase in suspended matter in the water column. The absence of birnessite is likely due to its rapid dissolution upon contact with H_2S in the pore water (Burdige and Nealson, 1986; Lenz et al., 2015). Given the strong spatial variability in H_2S concentrations near the sediment surface at site BY15 (Figs. 6 and 7), which is likely linked to the patchy occurrence of *Beggiatoaceae*, we expect that the distribution of birnessite was equally patchy. Thus, birnessite may have been present in the core used to determine the bulk geochemistry and likely was present in the surface sediments of the Eastern Gotland Basin.

The penetration of O_2 into the sediment led to major changes in its Mo, Fe and P geochemistry. Sediment Mo provides an excellent indicator for the oxidation state of the sediment (Scott and Lyons, 2012). Molybdenum occurs as molybdate (MoO_4^{2-}) in the water column, but when H_2S concentrations exceed $\sim$11 μM, complete conversion to tetrathiomolybdate (MoS_4^{2-}) and subsequent sequestration in the sediment is thought to occur (Helz et al., 1996; Erickson and Helz, 2000). Exposure of Mo-bearing sediments to O_2 rich bottom water results in the release of Mo to the pore water (Crusius et al., 1996). Our results indeed show such a release of Mo from the sediment into the pore water at site BY15 and site 1 as a consequence of bottom water re-oxygenation (Fig. 7). Our results further show that sedimentary Mo is highest at site BY15 and decreases along the transect with a decrease in water depth, becoming undetectable at the two shallowest sites 4 and 5 (Fig. 9). The comparatively high solid-phase Mo observed at the four deepest sites can be attributed to the euxinic conditions that prevailed in the deep bottom waters of the Eastern Gotland Basin prior to the recent MBIs (Fig. 2a).

The re-oxygenation led to distinct surface enrichments in labile Fe(III) oxides in the sediment at site BY15 and 1 (Fig. 9). These Fe oxide enrichments were $\sim$20-fold smaller than those in total Mn (Fig. 9). This difference can be partly explained by the 10- to 15-fold lower concentrations of Fe^{2+} in the water column prior to the re-oxygenation, when compared to Mn^{2+} (Section 4.1). As a consequence less Fe oxides than Mn oxides were formed upon re-oxygenation, leading to a smaller Fe oxide flux from the water column to the sediment. In addition, formation of Fe oxides from dissolved Fe^{2+} in the pore water was restricted by the high sulphide flux from the deeper sediment. We note that some Fe sulphides in the upper centimetre of the sediment may have been converted to Fe oxides. Importantly, we find little evidence for major downward oxidation of the sediment, as observed in other marine systems upon a bottom water redox change (Van Santvoort et al., 1996). We attribute this difference to the high upward fluxes of H_2S and NH_4^+ to the surface sediment and the corresponding high O_2 demand of the sediment (Table 3). When taking into account that two moles of O_2 are required to oxidize one mole of NH_4^+ or H_2S (Reed et al., 2011), it is evident that the O_2 flux into the sediment (0.5–4.9 mmol m^{-2} d^{-1}; Table 3) is currently insufficient to oxidize the upward flux of reductants at all sites (1.4–4.2 and 1.4–2.8 mmol m^{-2} d^{-1} for H_2S and NH_4^+, respectively; Table 3). This implies that H_2S and NH_4^+ will escape to the overlying water.

The oxidation of the surface sediments at site BY15, 1 and 2 led to enhanced P sequestration, as inferred from

Table 5
Proportion of water column P, Mn and Fe that was observed in the sediment.

	Phosphorus	Manganese	Iron
Calculated loss from the water column based on water column data	~232 mmol m^{-2}	~493 mmol m^{-2}	~103 mmol m^{-2}
Observed deposition onto the sediment based on sediment analysis	~12 mmol m^{-2}	~298 mmol m^{-2}	~11.5 mmol m^{-2}
Contribution of the sediment to total removal	5%	60%	11%

the surface enrichments in Ex-P + CDB-P (Figs. 10 and 11b). The sequential Ex-P step targets loosely sorbed P while the CDB-P targets Fe-oxide bound P. However, the observed P levels in the Ex-P + CDB-P extraction phases cannot solely be linked to Fe oxides. This is because the ratio of Fe oxides to Ex-P + CDB-P is ~1 (Figs. 9 and 10) whereas the lowest stoichiometric ratio that has been observed in marine environments for Fe oxides: P is ~2 (Gunnars et al., 2002). This implies that other minerals were co-extracted during the Ex-P + CDB-P steps in the SEDEX procedure. Phosphorus associated with $CaCO_3$ may be co-extracted during the SEDEX CDB-step (Kraal et al., 2017). However, $CaCO_3$ represents a minor pool (~2.5 wt%) in the sediments of the Eastern Gotland Basin, implying that P sequestration by $CaCO_3$ at our study sites is unlikely to be important. Previous studies of Baltic Sea sediments suggested that P associated with $MnCO_3$ minerals are also extracted in the SEDEX CDB step (Suess, 1979; Manheim, 1982; Jilbert and Slomp, 2013).

We indeed find that Mn enrichments in our sediments are strongly associated with P and Ca and not with Fe (Figs. 12 and 13; Supplementary Fig. S3). This coupling between Mn, P and Ca is further supported by the XANES spectra, which reveal the presence of $MnCO_3$ and Mn(II) phosphate minerals in these Mn-, Ca- and P-rich areas (Fig. 14). The Mn enrichments in the upper 0–0.6 mm of the surface sediment mainly consist of $MnCO_3$ minerals associated with P (Fig. 14a; Supplementary Fig. S3a). Based on the Mn spectra (Fig. 14), we observed a gradual transition from $MnCO_3$-P into Mn(II) phosphates ($Mn_3[PO_4]_2$) within the upper (0.5–4.8 mm) of the surface sediment (Fig. 13; Supplementary Fig. S3b). The presence of Mn(II) phosphates in coastal sediments was previously documented for the Bothian Sea (Egger et al., 2015). Manganese(II) phosphates have a high capacity to bind P and their resistance to reductive dissolution in the presence of H_2S will determine their contribution to the sequestration of P in the Baltic Sea. Below 7.5 mm depth in the surface sediment, the μXRF and XANES results indicate that Mn is primarily bound to pyrite and present in Mn-silicates (Figs. 13c and 14b). In summary, our results suggest a strong correlation between Mn, Ca and P in the surface sediment at site BY15 and a role for rhodochrosite and Mn(II) phosphates formation in P sequestration in the Eastern Gotland Basin.

The P sequestration associated with mineral formation in response to re-oxygenation was estimated from the change in solid-phase Ex-P + CDB-P (averaged over 2 cm sediment depth) between 2009 and 2016 (Fig. 11b). The details of the calculations are provided in the Supplementary Material, section 1.2. Here, we summarize the procedure. We first calculated the change in water column HPO_4^{2-} (~2.07 μM) upon re-oxygenation in the deeper water layer located below 125 m water depth based on the water column HPO_4^{2-} profiles (Fig. 3c). The deeper water layer below 125 m water depth contains 112,000 L per m^2 of sediment. Assuming that the ~2.07 μM change in HPO_4^{2-} in the deep water following the inflow was sequestered in the sediment, we calculate a total input of 232 mmol of P m^{-2} sediment. Applying the porosity (0.986) and sediment density (2.65 g cm^{-1}) this gives an average increase in concentration of Ex-P + CDB-P of 313 μmol P g^{-1} over 2 cm per m^2. However, the actual average increase in the Ex-P + CDB-P phase over the upper 2 cm per m^2 of the sediment as a result of re-oxygenation was only 16 μmol P g^{-1} (or 12 mmol P m^{-2}) which is equal to ~5% of the observed decline in water column HPO_4^{2}. Re-oxygenation of the water column thus had a limited impact on the removal of HPO_4^{2-} in the deeper waters of the Eastern Gotland Basin.

Similar calculations were made for Mn and Fe, as described in the Supplementary Material, section 1.3. Briefly, we used water column records for dissolved Mn for site BY15 from Dellwig et al. (2018) to estimate the loss of Mn from the water column following the re-oxygenation. For Fe, we used water column records from Pohl and Fernández-Otero (2012) to estimate the change in dissolved Fe. The surface enrichment in total Mn and Fe oxides at BY15 was assumed to be deposited from the water column. Based on these numbers, we estimate that at most 60% of the water column Mn and 11% of the water column Fe was sequestered in the sediment, as a consequence of the re-oxygenation (Table 5). Importantly, these metal oxides were not effective as scavengers of HPO_4^{2-} from the water column, since at most 5% of water column HPO_4^{2-} was sequestered in the sediment.

4.4. Implications

Previous work has shown that the increased accumulation of organic matter and Fe sulphides in sediments linked to hypoxia enhances the benthic O_2 demand (Turner et al., 2008; Reed et al., 2011). This 'legacy of hypoxia' may hinder return of a system to its previous state, i.e. the longer and more intense a period of hypoxia is, the more difficult recovery from hypoxia becomes because of the higher sediment O_2 demand (Turner et al., 2008). Our results show evidence for an upward flux of H_2S and NH_4^+ in the sediment that at the time of sampling outpaced benthic O_2 supply, thereby confirming such a 'legacy of hypoxia'.

Surface enrichments of Mn oxides and Fe oxides can act as a buffer for H_2S, restricting its release into the overlying water (Kristiansen et al., 2002; Kristensen et al., 2003). Based on the inventory of total Mn and Fe oxides in the surface sediment, we estimated that at site BY15, this amount of metal oxides could, buffer the H_2S for

approximately two months (71 days for Mn oxides, 3 days for Fe oxides; Supplementary Material, section 1.4). The duration of the buffering by Mn oxides was likely shorter, since a significant proportion of the Mn consisted of Mn(II) minerals. The first sampling of the Eastern Gotland Basin by SMHI took place 7 weeks after our sampling campaign and revealed the reoccurrence of euxinia (Fig. 2). This is in accordance with a time scale of buffering by metal oxides of days to weeks. We suggest that, as a consequence of the high flux of reductants, the natural ventilation events in the Eastern Gotland Basin only had a minor effect on the oxidation state of the sediment, allowing only a thin suboxic zone enriched in Fe oxides, Mn carbonates and Mn(II) phosphates to develop. Thus, the highly reducing conditions in sediments of the Eastern Gotland Basin currently limit the extent to which Mn, Fe and P are sequestered in mineral form in the sediment following re-oxygenation. While for Mn, this was previously recognized (Lenz et al., 2015; Häusler et al., 2018), the impact of the 'legacy of hypoxia' on Fe and P recycling upon re-oxygenation has so far not been well-described. We show here, for the first time, that the high flux of reductants from deeper sediment layers plays a role in restricting the penetration of O_2 into the sediment and thereby the formation of Fe oxides and associated P sequestration.

Our findings are of particular relevance to marine systems where a high P recycling contributes to a high productivity, as is the case in the present-day Baltic Sea (e.g. Gustafsson et al., 2012). Here, both the high O_2 demand and the limited P sequestration in the sediment act to minimize the biogeochemical impact of re-oxygenation events.

There have been calls to artificially ventilate the deep bottom waters in the Baltic Sea to reduce eutrophication (Stigebrandt and Gustafsson, 2007). Several pilot studies have been carried out in an anoxic fjord to stimulate the formation of Mn oxides and Fe oxides for the purpose of P sequestration (Viktorsson et al., 2013; De Brabandere et al., 2015; Stigebrandt et al., 2015). A critical assumption in such artificial ventilation attempts is that oxygenation always enhances P sequestration significantly. Thus, for example, Gustafsson and Stigebrandt (2007) estimated that the seafloor below 150 m water depth in the Baltic Sea may bind ~93 mmol P m^{-2} upon re-oxygenation. Here, we show that only ~ 12 mmol P m^{-2} is sequestered at site BY15 (Table 5), which we attribute to the highly reducing nature of the sediment and possibly the gradual decline in bottom water O_2 since the onset of re-oxygenation (Fig. 2). Since this 'legacy of hypoxia' currently strongly limits the formation of Mn- and Fe minerals in sediments and their capacity to sequester P, these artificial re-oxygenation projects that aim at removing water column HPO_4^{2-} and thereby improving water quality in the Baltic Sea will likely not have the desired outcome. Several modelling studies have shown that reducing P inputs to the Baltic Sea will eventually lead to a decline in water column HPO_4^{2-} and a decrease in the hypoxic area (Conley, 2012). Further reductions in P inputs from land thus are recommended over artificial re-oxygenation when aiming for an improvement of the water quality in the Baltic Sea.

5. CONCLUSIONS

The recent Major Baltic inflows in 2014 and 2015 mixed and partly replaced the deeper euxinic waters in the Eastern Gotland Basin with saline and oxygen-rich water from the North Sea. These natural ventilation events led to a rise in oxygen (O_2) and complete removal of sulphide (H_2S) in deeper waters. We show that re-oxygenation led to formation of the manganese (Mn) –oxide birnessite and Fe oxides in the water column and their deposition on the sediment. Only a relatively small proportion of the water column Mn (60%) and Fe (11%) was estimated to be sequestered in the sediment.

The exposure of the surface sediments to O_2-rich water induced the activity of sulphur-oxidizing bacteria belonging to the family *Beggiatoaceae* and an oxic and suboxic zone developed in the sediment at sites in the deeper part of the basin. In this thin surface layer, Fe oxides, Mn carbonates (and associated P), Mn(II) phosphates and possibly some Mn oxides accumulated.

Strikingly, our results indicate that the P sequestration linked to the recent inflows accounted for only ~5% of water column HPO_4^{2-} removal in the Eastern Gotland Basin, with most HPO_4^{2-} being displaced and transported to other parts of the basin. We attribute the limited sequestration of P to the highly reducing conditions in the sediment, which inhibited the formation of Fe oxides.

Our work shows that, the limited sequestration of P in the sediments of the Eastern Gotland Basin upon re-oxygenation forms an essential part of its 'legacy of hypoxia'. This finding is likely of relevance to many other euxinic basins subject to re-oxygenation. Finally, our research indicates that reducing nutrient inputs to the Baltic Sea is a better strategy when attempting to reduce the area of hypoxia/anoxia than artificial re-oxygenation.

ACKNOWLEDGEMENTS

We express our gratitude to the captain and crew of *R/V Pelagia* for their support during the expedition to the Baltic Sea in June 2016 (64PE411). We are grateful to S. Hidalgo-Martinez for assistance with the onboard microscopic analyses. This research was funded by the Netherlands Organisation for Scientific Research, Netherlands, Vici grant 865.13.005. Seventh Framework Programme, EU (European Union) and Formas (Sweden), BONUS COCOA grant 2112932-1. B. Gustafsson and E. Gustafsson were funded by the Swedish Agency for Marine and Water Management, Sweden, 1.11 Measure for Marine and Water environment. We thank T. Jilbert, H. de Waard, J.J Mulder and S. Ossebaar for analytical support. We are grateful to the European Synchrotron Radiation Facility (ESRF) for providing beam time at the Dutch-Belgium beamline (DUBBLE BM 26) in November 2016 and at the ID21 beamline (experiment ES-591) in May 2017. We thank the beamline scientists D. Banerjee, W. de Nolf and A.E. Pradas del Real for their assistance.

APPENDIX A. SUPPLEMENTARY MATERIAL

Supplementary data to this article can be found online at https://doi.org/10.1016/j.gca.2018.11.033.

REFERENCES

Adelson J., Helz G. and Miller C. (2001) Reconstructing the rise of recent coastal anoxia; molybdenum in Chesapeake Bay sediments. *Geochim. Cosmochim. Acta* **65**, 237–252.

Almroth-Rosell E., Eilola K., Kuznetsov I., Hall P. O. and Meier H. M. (2015) A new approach to model oxygen dependent benthic phosphate fluxes in the Baltic Sea. *J. Mar. Syst.* **144**, 127–141.

Altieri A. H., Harrison S. B., Seemann J., Collin R., Diaz R. J. and Knowlton N. (2017) Tropical dead zones and mass mortalities on coral reefs. *Proc. Natl. Acad. Sci.* **114**, 3660–3665.

Bartlett J. and Skoog D. (1954) Colorimetric determination of elemental sulfur in hydrocarbons. *Anal. Chem.* **26**, 1008–1011.

Berner R. A. (1980) *Early Diagenesis: A Theoretical Approach*. Princeton University Press.

Borsboom M. et al. (1998) The Dutch-Belgian beamline at the ESRF. *J. Synchotron Radiat.* **5**, 518–520.

Boudreau, B.P., 1997. Diagenetic models and their implementation.

Boyd P. and Ellwood M. (2010) The biogeochemical cycle of iron in the ocean. *Nat. Geosci.* **3**, 675.

Brewer P. and Spencer D. (1971) Colorimetric determination of manganese in anoxic waters. *Limnol. Oceanogr.* **16**, 107–110.

Brock J. and Schulz-Vogt H. N. (2011) Sulfide induces phosphate release from polyphosphate in cultures of a marine Beggiatoa strain. *ISME J.* **5**, 497–506.

Burdige D. J. (1993) The biogeochemistry of manganese and iron reduction in marine sediments. *Earth. Sci. Rev.* **35**, 249–284.

Burdige D. J. and Nealson K. H. (1986) Chemical and microbiological studies of sulfide-mediated manganese reduction. *Geomic. J.* **4**, 361–387.

Burton E. D., Bush R. T. and Sullivan L. A. (2006) Fractionation and extractability of sulfur, iron and trace elements in sulfidic wetland soils. *Chemosphere* **64**, 1421–1428.

Burton E. D., Sullivan L. A., Bush R. T., Johnston S. G. and Keene A. F. (2008) A simple and inexpensive chromium-reducible sulfur method for acid-sulfate soils. *Appl. Geochem.* **23**, 2759–2766.

Carstensen J., Andersen J. H., Gustafsson B. G. and Conley D. J. (2014a) Deoxygenation of the Baltic Sea during the last century. *Proc. Natl. Acad. Sci.* **111**, 5628–5633.

Carstensen J. et al. (2014b) Hypoxia in the Baltic Sea: biogeochemical cycles, benthic fauna, and management. *AMBIO* **43**, 26–36.

Claff S. R., Sullivan L. A., Burton E. D. and Bush R. T. (2010) A sequential extraction procedure for acid sulfate soils: partitioning of iron. *Geoderma* **155**, 224–230.

Cleceri L., Greenberg A. and Eaton A. (1998) Standard methods for the examination of water and wastewater. *APHA*.

Conley D. J. (2012) Ecology: save the Baltic sea. *Nature* **486**, 463.

Conley D. J., Humborg C., Rahm L., Savchuk O. P. and Wulff F. (2002) Hypoxia in the Baltic Sea and basin-scale changes in phosphorus biogeochemistry. *Environ. Sci. Technol.* **36**, 5315–5320.

Crusius J., Calvert S., Pedersen T. and Sage D. (1996) Rhenium and molybdenum enrichments in sediments as indicators of oxic, suboxic and sulfidic conditions of deposition. *Earth Planet. Sc. Lett.* **145**, 65–78.

Dale A. W., Bertics V. J., Treude T., Sommer S. and Wallmann K. (2013) Modeling benthic–pelagic nutrient exchange processes and porewater distributions in a seasonally hypoxic sediment: evidence for massive phosphate release by Beggiatoa? *Biogeosciences* **10**, 629–651.

De Baar H. J. et al. (2008) Titan: A new facility for ultraclean sampling of trace elements and isotopes in the deep oceans in the international Geotraces program. *Mar. Chem.* **111**, 4–21.

De Brabandere L. et al. (2015) Oxygenation of an anoxic fjord basin strongly stimulates benthic denitrification and DNRA. *Biogeochemistry* **126**, 131–152.

Dellwig O. et al. (2010) A new particulate Mn–Fe–P-shuttle at the redoxcline of anoxic basins. *Geochim. Cosmochim. Acta* **74**, 7100–7115.

Dellwig O., Schnetger B., Meyer D., Pollehne F., Häusler K. and Arz H. W. (2018) Impact of the major baltic inflow in 2014 on manganese cycling in the Gotland deep (Baltic Sea). *Front. Mar. Sci.* **5**, 248.

Diaz R. J. and Rosenberg R. (2008) Spreading dead zones and consequences for marine ecosystems. *Science* **321**, 926–929.

Dickson A. G. (1990) Standard potential of the reaction: AgCl (s) + $12H_2$ (g) = Ag (s) + HCl (aq), and the standard acidity constant of the ion HSO_4^- in synthetic sea water from 273.15 to 318.15 K. *J. Chem. Thermodyn.* **22**, 113–127.

Dickson A. G., Sabine C. L. and Christian J. R. (2007) *Guide to Best Practices for Ocean CO_2 Measurements*. North Pacific Marine Science Organization.

Egger M., Jilbert T., Behrends T., Rivard C. and Slomp C. P. (2015) Vivianite is a major sink for phosphorus in methanogenic coastal surface sediments. *Geochim. Cosmochim. Acta* **169**, 217–235.

Eilola K., Almroth-Rosell E. and Meier H. M. (2014) Impact of saltwater inflows on phosphorus cycling and eutrophication in the Baltic Sea: a 3D model study. *Tellus A* **66**, 23985.

Erickson B. E. and Helz G. R. (2000) Molybdenum (VI) speciation in sulfidic waters: stability and lability of thiomolybdates. *Geochim. Cosmochim. Acta* **64**, 1149–1158.

Goldhammer T., Brüchert V., Ferdelman T. G. and Zabel M. (2010) Microbial sequestration of phosphorus in anoxic upwelling sediments. *Nat. Geosci.* **3**, 557–561.

Grasshoff K. and Ehrhardt M. (1983) Automated Chemical Analysis. In *Methods of Seawater Analysis*. Verlag, pp. 263–289.

Gunnars A., Blomqvist S., Johansson P. and Andersson C. (2002) Formation of Fe (III) oxyhydroxide colloids in freshwater and brackish seawater, with incorporation of phosphate and calcium. *Geochim. Cosmochim. Acta* **66**, 745–758.

Gustafsson B. G. and Andersson H. C. (2001) Modeling the exchange of the Baltic Sea from the meridional atmospheric pressure difference across the North Sea. *J. Geophys. Res. Oceans* **106**, 19731–19744.

Gustafsson B. G. et al. (2012) Reconstructing the development of Baltic Sea eutrophication 1850–2006. *AMBIO* **41**, 534–548.

Gustafsson B. G. and Stigebrandt A. (2007) Dynamics of nutrients and oxygen/hydrogen sulfide in the Baltic Sea deep water. *J. Geosphys. Res Biogeosci.*, 112.

Hall P. O. et al. (2017) Influence of natural oxygenation of Baltic proper deep water on benthic recycling and removal of phosphorus, nitrogen, silicon and carbon. *Front. Mar. Sci.* **4**, 27.

Häusler K. et al. (2018) Massive Mn carbonate formation in the Landsort Deep (Baltic Sea): hydrographic conditions, temporal succession, and Mn budget calculations. *Mar. Geol.* **395**, 260–270.

Heiser U., Neumann T., Scholten J. and Stüben D. (2001) Recycling of manganese from anoxic sediments in stagnant basins by seawater inflow: a study of surface sediments from the Gotland Basin, Baltic Sea. *Mar. Geol.* **177**, 151–166.

Helz G. et al. (1996) Mechanism of molybdenum removal from the sea and its concentration in black shales: EXAFS evidence. *Geochim. Cosmochim. Acta* **60**, 3631–3642.

Holtermann P. L., Prien R., Naumann M., Mohrholz V. and Umlauf L. (2017) Deep-water dynamics and mixing processes during a major inflow event in the central Baltic Sea. *J. Geophys. Res. Oceans*.

Howarth R. et al. (2011) Coupled biogeochemical cycles: eutrophication and hypoxia in temperate estuaries and coastal marine ecosystems. *Front. Ecol. Environ.* **9**, 18–26.

Huckriede H. and Meischner D. (1996) Origin and environment of manganese-rich sediments within black-shale basins. *Geochim. Cosmochim. Acta* **60**, 1399–1413.

Ingall E. and Jahnke R. (1994) Evidence for enhanced phosphorus regeneration from marine sediments overlain by oxygen depleted waters. *Geochim. Cosmochim. Acta* **58**, 2571–2575.

Jeroschewski P., Steuckart C. and Kühl M. (1996) An amperometric microsensor for the determination of H_2S in aquatic environments. *Anal. Chem.* **68**, 4351–4357.

Jilbert T., de Lange G. and Reichart G. J. (2008) Fluid displacive resin embedding of laminated sediments: preserving trace metals for high-resolution paleoclimate investigations. *Limnol. Oceanogr-Meth.* **6**, 16–22.

Jilbert T., Slomp C., Gustafsson B. G. and Boer W. (2011) Beyond the Fe-P-redox connection: preferential regeneration of phosphorus from organic matter as a key control on Baltic Sea nutrient cycles. *Biogeosciences* **8**, 1699.

Jilbert T. and Slomp C. P. (2013) Iron and manganese shuttles control the formation of authigenic phosphorus minerals in the euxinic basins of the Baltic Sea. *Geochim. Cosmochim. Acta* **107**, 155–169.

Johnson K. S. et al. (2007) Developing standards for dissolved iron in seawater. *Eos, Trans. Am. Geophys. Union* **88**, 131–132.

Klunder M., Laan P., Middag R., De Baar H. and Van Ooijen J. (2011) Dissolved iron in the Southern Ocean (Atlantic sector). *Deep Sea. Res. Part 2* **58**, 2678–2694.

Koroleff F. (1969) Determination of ammonia as indophenol blue. *ICES*, 9.

Kraal P., Dijkstra N., Behrends T. and Slomp C. P. (2017) Phosphorus burial in sediments of the sulfidic deep Black Sea: key roles for adsorption by calcium carbonate and apatite authigenesis. *Geochim. Cosmochim. Acta* **204**, 140–158.

Kraal P. and Slomp C. P. (2014) Rapid and extensive alteration of phosphorus speciation during oxic storage of wet sediment samples. *PloS One* **9**, e96859.

Kraal P., Slomp C. P., Forster A., Kuypers M. M. and Sluijs A. (2009) Pyrite oxidation during sample storage determines phosphorus fractionation in carbonate-poor anoxic sediments. *Geochim. Cosmochim. Acta* **73**, 3277–3290.

Kristensen E., Kristiansen K. D. and Jensen M. H. (2003) Temporal behavior of manganese and iron in a sandy coastal sediment exposed to water column anoxia. *Estuaries* **26**, 690–699.

Kristiansen K., Kristensen E. and Jensen E. (2002) The influence of water column hypoxia on the behaviour of manganese and iron in sandy coastal marine sediment. *Estuar. Coast. Shelf Sci.* **55**, 645–654.

Lagerström M., Field M., Séguret M., Fischer L., Hann S. and Sherrell R. (2013) Automated on-line flow-injection ICP-MS determination of trace metals (Mn, Fe Co, Ni, Cu and Zn) in open ocean seawater: application to the GEOTRACES program. *Mar. Chem.* **155**, 71–80.

Lenz C., Behrends T., Jilbert T., Silveira M. and Slomp C. P. (2014) Redox-dependent changes in manganese speciation in Baltic Sea sediments from the Holocene Thermal Maximum: An EXAFS, XANES and LA-ICP-MS study. *Chem. Geol.* **370**, 49–57.

Lenz C., Jilbert T., Conley D., Wolthers M. and Slomp C. (2015) Are recent changes in sediment manganese sequestration in the euxinic basins of the Baltic Sea linked to the expansion of hypoxia? *Biogeosciences* **12**, 4875–4894.

Madison A. S., Tebo B. M., Mucci A., Sundby B. and Luther G. W. (2013) Abundant porewater Mn (III) is a major component of the sedimentary redox system. *Science* **341**, 875–878.

Malkin S. Y. et al. (2014) Natural occurrence of microbial sulphur oxidation by long-range electron transport in the seafloor. *ISME J.* **8**, 1843.

Manceau A., Marcus M. A. and Grangeon S. (2012) Determination of Mn valence states in mixed-valent manganates by XANES spectroscopy. *Am. Mineral.* **97**, 816–827.

Manheim F. T. (1982) Geochemistry of manganese carbonates in the Baltic Sea. *Stock. Contr. Geol.* **37**, 145–159.

Millero F. J., Plese T. and Fernandez M. (1988) The dissociation of hydrogen sulfide in seawater. *Limnol. Oceanogr.* **33**, 269–274.

Mohrholz V., Heene T., Beier S. and Naumann G. N. M. (2016) The impact of the recent series of barotropic inflows on deep water conditions in the Eastern Gotland Basin–time series observations. *Multiple Drivers for Earth System Changes in the Baltic Sea Region* **25**.

Mohrholz V., Naumann M., Nausch G., Krüger S. and Gräwe U. (2015) Fresh oxygen for the Baltic Sea—an exceptional saline inflow after a decade of stagnation. *J. Mar. Syst.* **148**, 152–166.

Mort H. P., Slomp C. P., Gustafsson B. G. and Andersen T. J. (2010) Phosphorus recycling and burial in Baltic Sea sediments with contrasting redox conditions. *Geochim. Cosmochim. Acta* **74**, 1350–1362.

Murphy J. and Riley J. P. (1962) A modified single solution method for the determination of phosphate in natural waters. *Anal. Chim. Acta* **27**, 31–36.

Neumann T., Radtke H. and Seifert T. (2017) On the importance of Major Baltic Inflows for oxygenation of the central Baltic Sea. *J. Geophys. Res. Oceans* **122**, 1090–1101.

Nikitenko S. et al. (2008) Implementation of a combined SAXS/WAXS/QEXAFS set-up for time-resolved in situ experiments. *J. Synchotron Radiat.* **15**, 632–640.

Noffke A., Sommer S., Dale A., Hall P. and Pfannkuche O. (2016) Benthic nutrient fluxes in the Eastern Gotland Basin (Baltic Sea) with particular focus on microbial mat ecosystems. *J. Mar. Syst.* **158**, 1–12.

Obata H., Karatani H. and Nakayama E. (1993) Automated determination of iron in seawater by chelating resin concentration and chemiluminescence detection. *Anal. Chem.* **65**, 1524–1528.

Pohl C. and Fernández-Otero E. (2012) Iron distribution and speciation in oxic and anoxic waters of the Baltic Sea. *Mar. Chem.* **145**, 1–15.

Poulton S. W. and Canfield D. E. (2005) Development of a sequential extraction procedure for iron: implications for iron partitioning in continentally derived particulates. *Chem. Geol.* **214**, 209–221.

Raiswell R. and Canfield D. E. (2012) The iron biogeochemical cycle past and present. *Geochem. Perspect.* **1**, 1–2.

Raiswell R., Vu H. P., Brinza L. and Benning L. G. (2010) The determination of labile Fe in ferrihydrite by ascorbic acid extraction: methodology, dissolution kinetics and loss of solubility with age and de-watering. *Chem. Geol.* **278**, 70–79.

Ravel B. and Newville M. (2005) ATHENA, ARTEMIS, HEPHAESTUS: data analysis for X-ray absorption spectroscopy using IFEFFIT. *J. Synchotron. Radiat.* **12**, 537–541.

Reed D. C., Slomp C. P. and Gustafsson B. G. (2011) Sedimentary phosphorus dynamics and the evolution of bottom-water hypoxia: a coupled benthic–pelagic model of a coastal system. *Limnol. Oceanogr.* **56**, 1075–1092.

Reissmann J. H. et al. (2009) Vertical mixing in the Baltic Sea and consequences for eutrophication–a review. *Prog. Oceanogr.* **82**, 47–80.

Rijkenberg M. J. et al. (2015) "PRISTINE", a new high volume sampler for ultraclean sampling of trace metals and isotopes. *Mar. Chem.* **177**, 501–509.

Rijkenberg M. J. et al. (2014) The distribution of dissolved iron in the West Atlantic Ocean. *PloS One* **9**, e101323.

Rosenberg R., Magnusson M. and Stigebrandt A. (2016) Rapid re-oxygenation of Baltic Sea sediments following a large inflow event. *AMBIO* **45**, 130.

Ruttenberg K. C. (1992) Development of a sequential extraction method for different forms of phosphorus in marine sediments. *Limnol. Oceanogr.* **37**, 1460–1482.

Salomé M. et al. (2013) The ID21 scanning X-ray microscope at ESRF. *J. Phys. Conf. Ser.* **425**, 182004.

Schlitzer, R., 2015. Ocean Data View.

Schmidtko S., Stramma L. and Visbeck M. (2017) Decline in global oceanic oxygen content during the past five decades. *Nature* **542**, 335–339.

Schneider B. (2011) PO_4 release at the sediment surface under anoxic conditions: a contribution to the eutrophication of the Baltic Sea? *Oceanologia* **53**, 415–429.

Scott C. and Lyons T. W. (2012) Contrasting molybdenum cycling and isotopic properties in euxinic versus non-euxinic sediments and sedimentary rocks: Refining the paleoproxies. *Chem. Geol.* **324**, 19–27.

Seitaj D. et al. (2015) Cable bacteria generate a firewall against euxinia in seasonally hypoxic basins. *Proc. Natl. Acad. Sci.* **112**, 13278–13283.

Slomp C. P., Epping E. H., Helder W. and Raaphorst W. V. (1996) A key role for iron-bound phosphorus in authigenic apatite formation in North Atlantic continental platform sediments. *J. Mar. Res.* **54**, 1179–1205.

Soetaert, K., Petzoldt, T., Meysman, F., 2010. Marelac: Tools for Aquatic Sciences. R Package Version.

Solé V., Papillon E., Cotte M., Walter P. and Susini J. (2007) A multiplatform code for the analysis of energy-dispersive X-ray fluorescence spectra. *Spectrochim. Acta B* **62**, 63–68.

Sommer S. et al. (2017) Major bottom water ventilation events do not significantly reduce basin-wide benthic N and P release in the Eastern Gotland Basin (Baltic Sea). *Front. Mar. Sci.* **4**.

Steenbergh A. K., Bodelier P. L., Slomp C. P. and Laanbroek H. J. (2014) Effect of redox conditions on bacterial community structure in Baltic Sea sediments with contrasting phosphorus fluxes. *PloS One* **9**, e92401.

Stigebrandt A. and Gustafsson B. G. (2007) Improvement of Baltic proper water quality using large-scale ecological engineering. *AMBIO* **36**, 280–286.

Stigebrandt A. et al. (2015) An experiment with forced oxygenation of the deepwater of the anoxic By Fjord, western Sweden. *AMBIO* **44**, 42–54.

Stigebrandt A., Rosenberg R., Magnusson M. and Linders T. (2017) Oxygenated deep bottoms beneath a thick hypoxic layer lack potential of benthic colonization. *AMBIO*, 1–4.

Strickland, J.D., Parsons, T.R., 1972. A practical handbook of seawater analysis.

Suess E. (1979) Mineral phases formed in anoxic sediments by microbial decomposition of organic matter. *Geochim. Cosmochim. Acta* **43**, 339343–341352.

Sulu-Gambari F., Roepert A., Jilbert T., Hagens M., Meysman F. J. and Slomp C. P. (2017) Molybdenum dynamics in sediments of a seasonally-hypoxic coastal marine basin. *Chem. Geol.* **466**, 627–640.

Sulu-Gambari F., Seitaj D., Behrends T., Banerjee D., Meysman F. J. and Slomp C. P. (2016a) Impact of cable bacteria on sedimentary iron and manganese dynamics in a seasonally-hypoxic marine basin. *Geochim. Cosmochim. Acta* **192**, 49–69.

Sulu-Gambari F., Seitaj D., Meysman F. J., Schauer R., Polerecky L. and Slomp C. P. (2016b) Cable bacteria control iron–phosphorus dynamics in sediments of a coastal hypoxic basin. *Environ. Sci. Technol.* **50**, 1227–1233.

Teske A. and Nelson D. C. (2006) The genera Beggiatoa and Thioploca. In *The Prokaryotes*. Springer, pp. 784–810.

Turner R. E., Rabalais N. N. and Justic D. (2008) Gulf of Mexico hypoxia: alternate states and a legacy. *Environ. Sci. Technol.* **42**, 2323–2327.

Turnewitsch R. and Pohl C. (2010) An estimate of the efficiency of the iron-and manganese-driven dissolved inorganic phosphorus trap at an oxic/euxinic water column redoxcline. *Glob. Biogeochem Cycl.*, 24.

Vahtera E. et al. (2007) Internal ecosystem feedbacks enhance nitrogen-fixing cyanobacteria blooms and complicate management in the Baltic Sea. *AMBIO* **36**, 186–194.

Van Santvoort P. et al. (1996) Active post-depositional oxidation of the most recent sapropel (S1) in sediments of the eastern Mediterranean Sea. *Geochim. Cosmochim. Acta* **60**, 4007–4024.

Van Santvoort P. J. M., De Lange G., Thomson J., Colley S., Meysman F. and Slomp C. (2002) Oxidation and origin of organic matter in surficial Eastern Mediterranean hemipelagic sediments. *Aquat. Geochem.* **8**, 153–175.

Viktorsson L., Kononets M., Roos P. and Hall P. O. (2013) Recycling and burial of phosphorus in sediments of an anoxic fjord-the By Fjord, western Sweden. *J. Mar. Res.*.

Yakushev E., Kuznetsov I., Podymov O., Burchard H., Neumann T. and Pollehne F. (2011) Modeling the influence of oxygenated inflows on the biogeochemical structure of the Gotland Sea, central Baltic Sea: changes in the distribution of manganese. *Comput. Geosci.* **37**, 398–409.

Yücel M., Sommer S., Dale A. W. and Pfannkuche O. (2017) Microbial sulfide filter along a benthic redox gradient in the Eastern Gotland Basin, Baltic Sea. *Front. Microbiol.* **8**, 169.

Associate editor: Orit Sivan